SIRKISOON, LEONA RAVINI, M.S. Structural Characterization and Docking Studies of Acetylcholine Binding Proteins. (2009)
Directed by Dr. Patricia H. Reggio. 56pp.

Neuronal Nicotinic Receptors (NNRs) are ligand gated ion channels located both pre- and postsynaptically in the peripheral and central nervous systems. NNRs are important pharmaceutical targets for schizophrenia, pain, epilepsy, tobacco dependence, Tourette's syndrome, Alzheimer's disease, Parkinson's disease, myasthenia gravis, and depression.[1, 2] Rational drug design for NNRs has been hampered by the lack of crystallographic information about this important target. Currently, there exist two atomic-level structures representing NNR subtypes. The first a cryoelectron micrograph of a muscle NNR[3] at 4 Å resolution provided initial structural information about the complete receptor. A more recent crystal structure of the extracellular domain of the mouse nicotinic acetylcholine receptor (NNR) α1 subunit bound to α-bungarotoxin at 1.94 Å resolution is the first atomic-resolution view of a NNR subunit extracellular domain.[2] Other receptor structural data has arisen from acetylcholine binding proteins (AChBPs) [4, 5] isolated from freshwater and marine snails. AChBPs are water-soluble proteins, which are homologues of the extracellular domain of the NNRs.

Information collected during this project will be used to aid in the development of homology models for various NNR subtypes, based on a more complete understanding of AChBPs. To this end, available co-crystal structures were analyzed through measurement of distances and angles between residues that make up the ligand binding domain (LBD). Further, to evaluate the utility of various docking/scoring algorithms docking studies were performed on these AChBP co-crystal structures. Nineteen NNR ligands were docked into the AChBPs using Schrodinger's Glide 5.0 software.

A few of the key findings of this research are as follows. First, careful examination of the various geometric parameters shows that large changes occur to the AChBP LBD as a ligand binds. These changes include a 15 residue C-loop closing over the LBD with a concomitant movement of the two subunits that make up the LBD relative to each other to accommodate the ligand. The latter is illustrated by changes in the chi 1 and chi 2 of tyrosine (Y) 55 (from the complementary face) and changes in the chi 1 of tyrosine (Y) 93 in the lobeline AChBP to make room in the LBD for one of the phenyl rings on lobeline. Second, results from the docking studies on all available AChBP-co-crystal structure suggest that the AChBP lobeline structure is the best template for homology modeling based on the following: (1) Glide 5.0 was able to dock most of a diverse set of 19 NNR ligands into this structure, in contrast to more limited success for other AChBP starting points; (2) in cases where the crystal structure had been determined, poses similar to those found for the actual co-crystal structure could be reproduced; (3) the correlation between the Glide score (Gscore) for these expected poses and experimental pK_d values was (while still modest) best for this structure (correlation, 0.30); (4) correlation between the best Gsore and the pK_d was highest for the lobeline AChBP structure (R^2 = 0.38). The lobeline AChBP structure is now under investigation as a template to generate homology models to aid in drug discovery at Targacept.

STRUCTURAL CHARACTERIZATION AND DOCKING STUDIES

OF ACETYLCHOLINE BINDING PROTEINS

By

Leona Ravini Sirkisoon

A Thesis Submitted to
the Faculty of The Graduate School at
The University of North Carolina at Greensboro
in Partial Fulfillment
of the Requirements for the Degree
Master of Science

Greensboro
2009

Approved by

_____
Committee Chair

APPROVAL PAGE

This thesis has been approved by the following committee of the Faculty of The Graduate School at The University of North Carolina at Greensboro.

Committee Chair _____
Patricia H. Reggio

Committee Members _____
Philip S. Hammond

_____
J. Phillip Bowen

April 28th, 2009
_____
Date of Acceptance by Committee

April 13th, 2009
_____
Date of Final Oral Examination

ACKNOWLEDGEMENTS

I would like to thank Dr. Patricia H. Reggio, Dr. Philip S. Hammond and Dr. J. Phillip Bowen for all the help provided and for serving on my committee. I would also like to thank Targacept Inc. for providing assistantship support for this work.

TABLE OF CONTENTS

LIST OF TABLES

Page

LIST OF FIGURES

Page

CHAPTER I

LITERATURE REVIEW

Importance of Neuronal Nicotinic Receptors

Nicotinic acetylcholine receptors (NNRs) are transmembrane cation channels and members of the ligand gated ion channel (LGIC) family.[4,3] NNRs mediate cationic flux across cell membranes,[4] allowing sodium (Na^+), potassium (K^+) and calcium (Ca^{2+}) ions to flow into the cell but not out.[3,6] NNRs function by depolarizing the cell membrane, with subsequent activation of K^+ channels.[7,8] NNRs are found in ganglia and in neuromuscular junctions, as well as in the central nervous system (CNS),[3,2] are made up of five subunits, and exist as both hetero- and homopentamers. A variety of different subunit types have been identified, designated α2-α10, β2-β4, γ and δ/ε[6] and these may combine in a variety of ways, leading to a number of receptor subtypes based on various subunit combinations.

NNRs are activated by the endogenous neurotransmitter acetylcholine, by the prototypical ligand nicotine as well as by other agonists. Ligand binding of agonists and antagonists occurs at the outside midsection of the extracellular domain (ECD), with resulting pore opening and ion flow through the channel, or blockade of the receptor.[3] Based on their extensive anatomical distribution and their ability to pre-synaptically modulate a variety of signaling processes, neuronal nicotinic receptors (NNRs) are a target for drug discovery because of their potential to impact various CNS diseases and

disorders. NNRs have been extensively validated as therapeutic targets for various CNS pathologies such as schizophrenia, anxiety, epilepsy, depression, analgesia, addiction disorders, Alzeihmer disease, Parkinson disease and inflammation.[1,9,10,11] Chantix®, a compound targeted at the human $\alpha 4\beta 2$ receptor, is currently on the market (Pfizer) for smoking cessation.

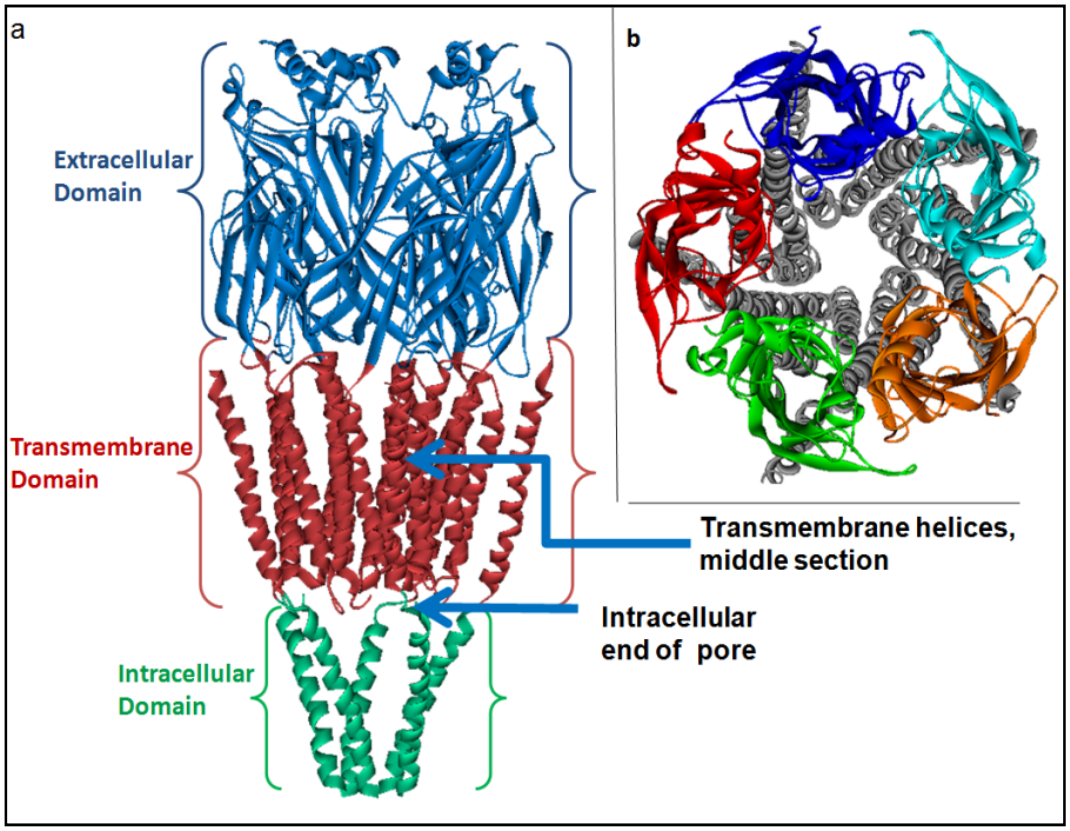

Figure 1. *Torpedo mamorata* Nicotinic Receptor Side and Top View. Similar to image in Unwin, N. *J. Mol. Biol.* 2005, 346, 967-989. **a:** extracellular, transmembrane and intracellular domains, and possible gate locations. **b:** receptor viewed from the extracellular domain and looking down the pore opening, with views for the five different subunits.

Crystal Structures Available

Currently, there exist two atomic-level structures representing nicotinic receptor subtypes, a 4 Å resolution of the heteropentameric muscle-type receptor shown in Figure 1[3] and a single α1 subunit at 1.94 Å resolution.[2] Structurally, in addition to the ligand-binding site where competitive agonists and antagonists interact, there are several other areas of interest in the receptor structure. Evidence suggests that the ion channel gate may be located in two possible locations: the middle of the transmembrane helices (TMH); or, at the intracellular end of the pore (Figure 1a).[12] Further, allosteric modulators (both potentiators and inhibitors) are an important class of ligands that interact with the NNRs, perhaps at several sites non-concurrent with the competitive agonist and antagonist site.

Other receptor structural data has arisen from acetylcholine binding proteins (AChBPs),[13] water soluble homologues of the NNRs ECD. These proteins, like the homopentameric NNRs, show five separate ligand binding domains (LBDs) and interact with NNR ligands, as shown by co-crystallization with both NNR agonists and antagonists.[4,5] AChBPs have been isolated from *Lymnaea stagnalis* (Great Pond Snail), *Aplysia californica* (California Sea Hare) and *Bulinus truncatus,* L-, A- and B-AChBP respectively.[13,4,5,14] To date, only the Aplysia and Lymnaea AChBPs have been co-crystallized with NNR ligands. It is also of note that coupling a modified version of L-AChBP with the transmembrane region of the 5-HT_{3A} receptor was reported to provide a functional NNR analog.[15]

Sequence Alignment

Overall, AChBPs show only modest sequence similarity to LGICs (15-28%)[4] but do show very similar characteristics to the NNR LBDs. Sequence alignment of L- , B- and A-AChBP, along with the α4, β2 and α7 subunits of the human NNRs are shown in Figure 2. The sequence alignment was generated using Clustal W from San Diego Supercomputer Center (SDSC) Biology Workbench.

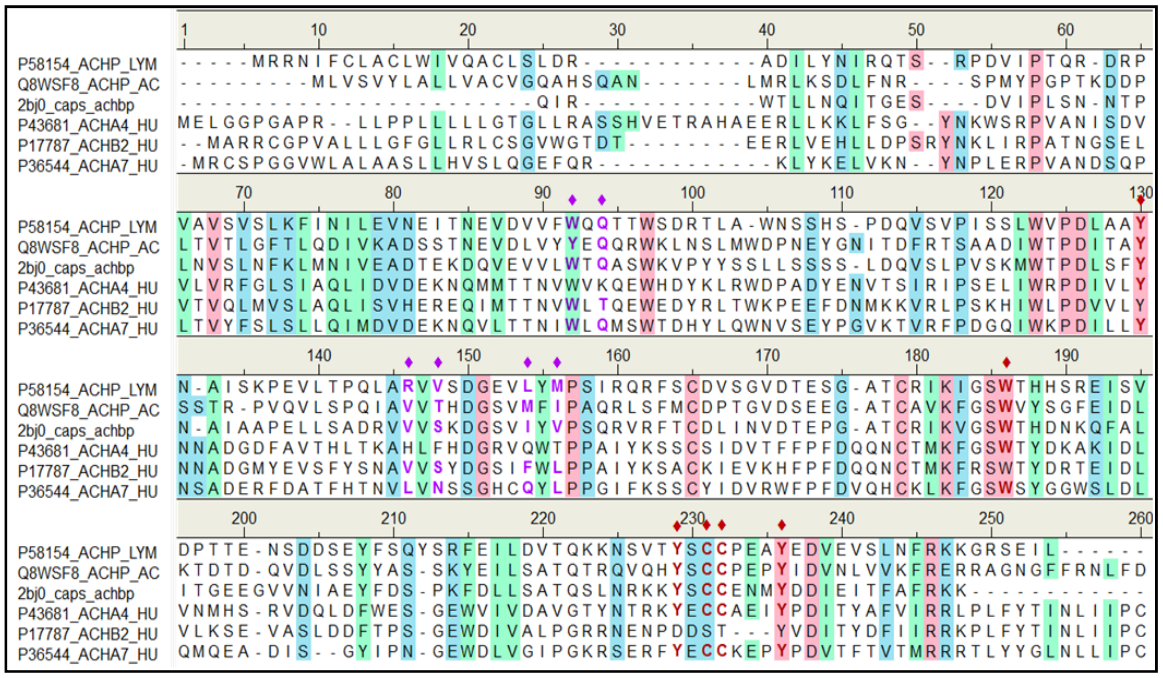

Figure 2. Sequence Alignment. Sequence alignment between Lymnaea, Aplysia and Bulinus AChBP and Human α4, α7 and β2 subunits. Identical, strongly similar and weakly similar residues are identified by pink, green and blue backgrounds, respectively. A white background designates nonmatching residues. The LBD residues are marked by a diamond with red diamonds indicating the residues on the principal face and purple diamonds from the complementary face.

Acetylcholine Binding Protein and Neuronal Nicotinic Receptor Comparison

Based on co-crystal structures as well as an apo form of the aplysia AChBP (where the LBDs are weakly occupied[5]) the LBDs can be thought of as existing in various "states", states that depend on the ligand's structure and function at different NNRs. Further, when all five LBDs are occupied by the same ligand in a crystal structure, or when only some but not all of the LBDs are occupied, additional information on differences from one LBD to another may be examined. Therefore, these occupied LBDs may be compared to unoccupied LBDs in either the same crystal structure or the apo form[5] to provide data on the effect of various agonists and antagonists on the LBD geometry. These data may provide useful information of use for the development of homology models for the NNRs.

A number of features play critical roles for ligand binding in the AChBPs. These include the B-loop and the C-loop (containing a sulfur-sulfur bond in adjacent cysteine-cysteine residues) from one subunit , and the F-Loop from another subunit(Figure 3).[5]

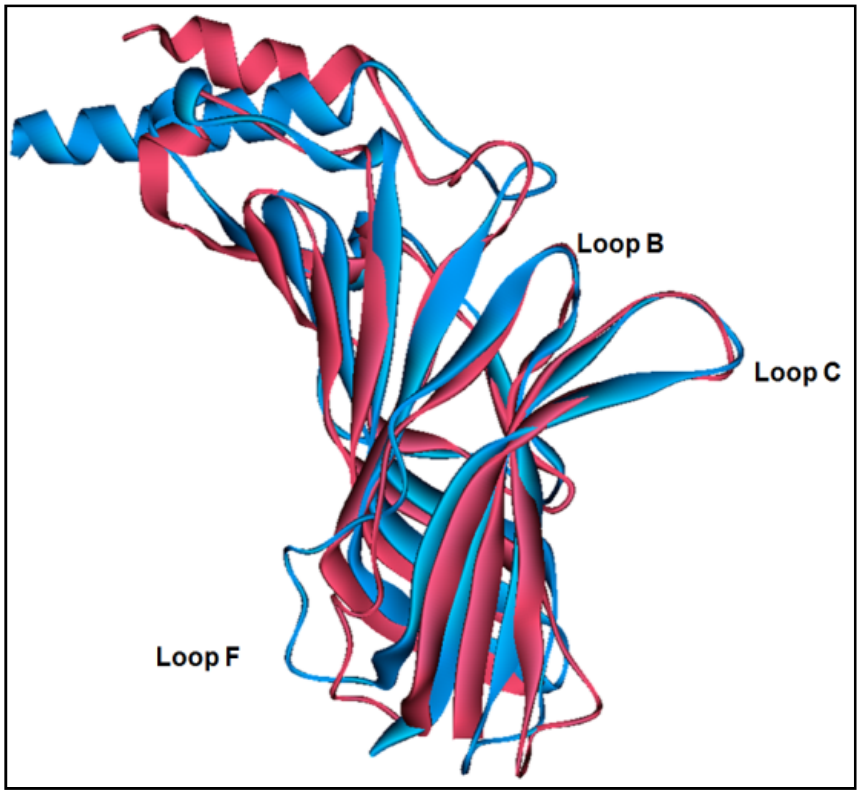

Figure 3. Nicotinic Receptor and Apo AChBP Monomer Comparison. Similar to image in Hansen, S. B.;et al.. The Embo Journal. 2005, 24, 3635-3646. One subunit of the apo AChBP (blue) superimposed on one subunit of the torpedo (red) structure. Loops that participated in ligand binding are named.

The LBDs for all AChBPs (and NNRs) are composed of the C-Loop from one face (called the principal face) and the residues that come in contact with the C-loop on the adjacent face (called the complementary face).[5] Ligands co-crystallized with the AChBPs represent considerable diversity in shape and size, with the crystallographic data showing significant variance in the LBD depending on the ligand co-crystallized. For example, the C-Loop can move as much as 11 Å depending on the ligand that is bound. It moves 7.3 Å inward from the apo[5] form when a small agonist like epibatidine binds and 4.3 Å outward from the apo form to open up for interaction with the peptide antagonist α-connotoxin.[5]

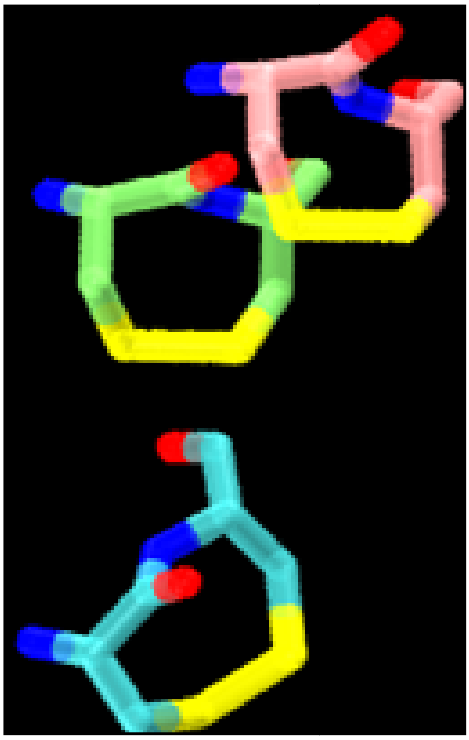

Figure 4. C-Loop Movement. Similar to part of an image in Hansen, S. B.;et al. The Embo Journal. 2005, 24, 3635-3646. Shows representative movements of the "top" of the C-Loop in comparisons of epibatidine AChBP (blue), the apo form of A-AChBP (green) and the a-connotoxin A-AChBP (red) structures.

The *Aplysia californica* AChBP has been co-crystallized with a variety of ligands from the agonists epibatidine and lobeline to the antagonists methyllycaconitine and the small peptide, α-connotoxin.[5] For AChBP from *Lymnaea stagnalis*, two co-crystal structures with two agonists, nicotine and carbamylcholine[4] have been published. The large movements in the C-loop result in small changes of less than 2 Å of other loops near the C-terminal transmembrane region.[5] Hansen and colleagues propose that the NNRs mimic the molecular motions observed by AChBPs which may lead to channel gating.[5] Receptor structural data also comes from a cryoelectron micrograph of *Torpedo mamorata* and the α1 face of a mouse muscle NNR.[3,2]

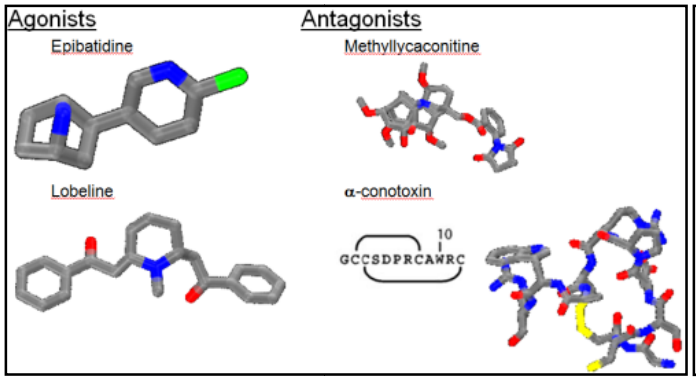

Figure 5. Ligands co-crystallized with Aplysia AChBP.

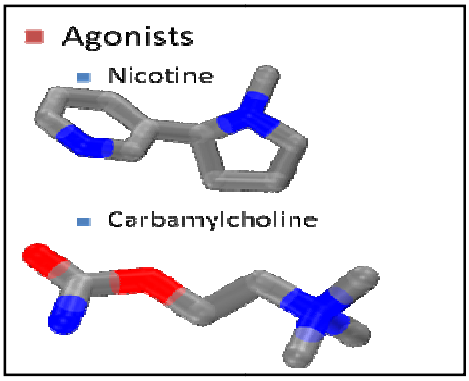

Figure 6. Ligands co-crystallized with Lymnaea AChBP.

Careful analysis of the nicotine, carbamylcholine and hepes co-crystal structures reveal that the cationic center of the protonated or quaternary amine ligand is located above tryptophan 143 (W143 in the Lymnaea structure and W147 in the Aplysia AChBP) forming a cation-π interaction. Tryptophan displays the strongest cation-π binding interaction of all the naturally occurring aromatic amino acids.[16] Artali and colleagues propose that electrostatic and steric interactions control the stability of the ligand-protein complex in ACHBP, and that the cation-π interaction is most important, especially for NNR activity.[17] For NNRs, it is also expected that the endogenous neurotransmitter, acetylcholine to bind through a cation-π interaction with its quaternary amine and the electron rich aromatic side chains of the LBD.[17]

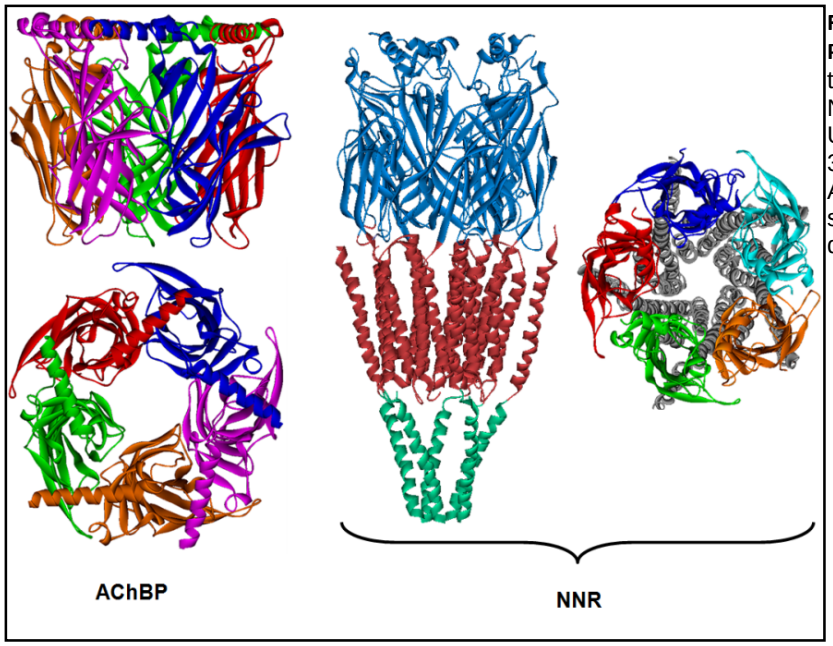

Figure 7. Apo AChBP and NNR Pentamer Comparison. Similar to image in Brejc, K.; et. al. Nature. 2001, 411, 269-276, Unwin, N. J. Mol. Biol. 2005, 346, 967-989. Not that the AChBP structure is very similar to the extracellular domain of the NNR.

To better understand the effects of ligand binding on the relative geometry of residues located in the LBD, I undertook a careful analysis of both intra- and inter-variations in structure for the L- and A-AChBPs that have been co-crystallized with NNR ligands. Further, examined the ability of several docking algorithms to reproduce the known poses (based on crystallographic data) of co-crystallized NNR ligands, and the ability of scoring functions to accurately reproduce ligand binding affinities for a divers set of NNR ligands.

CHAPTER II

INTRODUCTION

Hypotheses

Geometric analysis of the five LBDs in AChBPs should provide data on the extent of vaience from one LBD to another within a single protein while analysis of different co-crystal structures as well as the apo form should provide information on those changes that occur as a result of ligand binding. The five LBDs in a single protein are expected to be quite similar, while dramatic differences are expected for different ligands, as well as the apo[5] form. A more complete understanding of the LBDs and changes that occur after ligand binding will provide a better understanding of how various ligands interact with LBD residues, and should provide a basis for the development of better homology models of NNRs.

CDOCKER and Glide 4.5 (standard precision and extra precision) docking algorithms should reproduce the crystal structure pose for the ligands that are co-crystallized, and their scoring functions should rank order the poses in terms of RMSD (the pose that is closest to the co-crystal structure pose should have one of the best scores). Therefore a correlation between the scores and RMSD should exist. However, since the NNR ligands bind through a cation-π interaction[17] and the scoring functions for CDOCKER and Glide 4.5 (standard precision and extra precision) do not reward this type of interaction, the scoring functions do not correlate with the RMSD. The information from these experiments will be used to pick a few proteins and a single

method to run docking studies on a variety of NNR ligands with known K_d values to examine the correlation between K_d values and scores for various poses.

Goals

Ultimately, data collected during this project will help guide development of homology models for various NNR subtypes, based on a more complete understanding of AChBPs. These homology models may then be used to guide drug discovery efforts. To achieve this goal, the following tasks will be undertaken:

1. The AChBPs LBD for the different ligands that have been co-crystallized will be geometrically analyzed.
2. Several different docking tools and scoring functions will be explored using the nicotine (nic),[4] carbamylcholine (cce),[4] apo,[5] epibatidine (epi),[5] methyllycaconitine (mla)[5] and lobeline (lob)[5] crystal structures as docking structures. A scoring function will be sought that correlates with known AChBP experimental binding data (Kd).
3. Determine which of the co-crystal structure AChBPs provides the lowest RMSD for docked NNR compounds and which docking tool show most promise in reproducing either the RMSD and/or correlates best with docking scores.

CHAPTER III

PROCEDURES

Aim 1. AChBP Geometrical Analysis Using Maestro V 7.5 (Schrodinger, Inc.) and Discovery Studio 2.0 (Accelrys)

Protein Structural Data: PDB codes for Aplysia AChBP are 2BYN (APO), 2BYR (MLA co-crystal structure) 2BYS (LOB co-crystal structure)and 2BYQ (EPI co-crystal structure).[5] PDB codes for Lymnaea AChBP are 1UV6 (CCE co-crystal structure) and 1UW6 (nicotine co-crystal structure).[4]

Protein Sequence Analysis: To illustrate the similarities and differences both across the three AChBP proteins, and their similarities and differences to the NNR extracellular regions, sequence alignment of A-, L- and B-AChBP with human $\alpha 4, \beta 2,$ and $\alpha 7$ subtypes were carried out. This was done using Clustal W multiple sequence alignment which is available through Biology workbench version 3.2 offered by the SDSC (San Diego Supercomputer Center). All the default settings were used. This sequence alignment was done in order to compare the three AChBP structures with both human and rat $\alpha 3$-$\alpha 7$ and $\beta 2$-$\beta 4$. The alignments for some of the subtypes were removed for clarity.

Geometric Protein Analysis: To better characterize the subtle differences that exist both within crystal structures of the various AChBP structures and across the various co-crystal structures, centroids were defined for all key residues in the LBD.

Measurements were taken for distances from the centroid of the binding site residues to each other (including the ring formed by C190 and C191) from different co-crystal structures. These distances were measured for each of the five potential binding sites, using Maestro 7.5 and then the average and standard deviation values for each distance were calculated and graphed relative to the apo form[5]. This provides a snapshot of both consistency within a structure and variation across structures for various geometric features that help define the pharmacophoric recognition feature of the LBD. In addition, angles (defined to illustrate key features in the LBD) were also measured for each binding site, as were Chi1 and Chi2 parameters for each aromatic residue. The Chi1 and Chi2 parameters were measured using the MOE program from Chemical Computing Group. Averages and standard deviations were calculated for each angle and graphed. In this case the angles were not relative to the apo form. Since each LBD is formed through interactions of two subunits, pharmacophoric distances were measured between I118 and W147 to indicate the movement of each subunit relative to each other. This distance was measured using Discovery Studio 2.0 from Accelrys.

Ligand-Protein Analysis: Analyses were performed to determine changes that occur when both agonists and antagonists bind to the AChBP. Distances from the cationic center to the centroid of the aromatic rings of the binding site were measured for several co-crystal structures. Angles and torsions were also measured. As a visual indicator of variance, distances were plotted on one graph while angles and torsions were plotted on separate graphs. The angles measured were:

- Cationic center → W147 centroid → the N of the indole ring on W147; this angle provides a measure of the relative alignment of the ligand cationic center to the conserved tryptophan.

- For L-AChBP structures, cationic center→W55centroid→the N of the indole ring on W55. For A-AChBP, W55 is replaced by tyrosine. In the latter case, the carbon atom of the tyrosine ring closest to the indole N from W55 was used, with that atom determined by superimposition of the lymnaea and aplysia structures using backbone atoms. This angle provides an indication of movement of the complementary face relative to the principal face.

In order to determine the position of the ligand in the binding site relative to the conserved tryptophan (W147), two torsion angles were measured:

- W147 indole ring N→W147centroid→cationic center→W147 backbone carbonyl
- W147 indole ring N→W147centroid→cationic center→ligand hydrogen bond acceptor

Ligand protein analyses were carried out on all 5 of the binding sites in the epibatidine (A-AChBP) and nicotine (L-AChBP) co-crystal structures in order to measure variation from one LBD to the next.

Aim 2. AChBP Docking Studies

Hansen et al.[5] have observed that each ligand co-crystalized with an AChBP induces local conformational changes. Further, the C-loop acts as an "induced-fit sensor" which effectively molds itself around the ligand during binding. Based on these observations, studies were undertaken to dock co-crystal structure ligands both back into their complimentary LBD, but also into the LBDs of other AChBPs (both from aplysia and lymenaea). These studies were designed to assess how sensitive docking algoritms might be to these local changes. Further, there was the question of templates for

binding studies – was one structure more likely than another to serve as a satisfactory starting point for correlation with binding affinity values.

Structures selected for these studies are shown in Table 1 along with binding affinity values for L-AChBP and/or A-AChBP. Kd values are taken from the literature or from private communications from Dr. Todd T. Talley, University of California, San Diego.

Table 1. NNR Ligand Dataset. Name, structure and Kd values for both Lynmaea and Aplysia AChBPs. The two sterioisomers of nicotine and TI-1 were docked because both bind to the receptor.

Structures	Name	Kd (nM) Ls	Kd (nM) Ac		Structures	Name	Kd (nM) Ls	Kd (nM) Ac
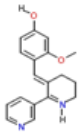	2MeO4OHBA[a]	0.43	3		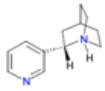	TI-3_S[d]	41	384
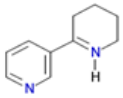	Anabaseine[a]	240	1001		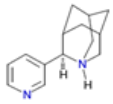	TI-4[d]	49	563
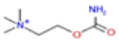	Carbamylcholine[b]	7575	ND		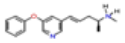	TI-5[d]	1025	13000
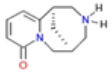	Cytisine[d]	480	2926		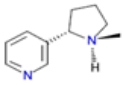	Nicotine_SR[a]	100	260
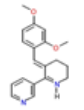	DMXBA[a]	19	330		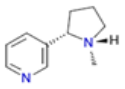	Nicotine_SS[a]	100	260
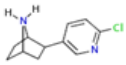	Epibatidine[a]	0.3	8.6		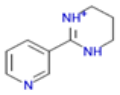	PTHP[a]	220	1001
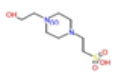	Hepes[d]	265	ND		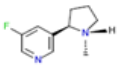	TI-1_RS[d]	3738	35055
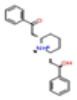	Lobeline_SRRR[c]	130	0.5		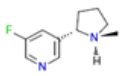	TI-1_SR[d]	3738	35055
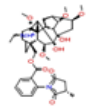	Methyllycaconitine[c]	0.4	2.8		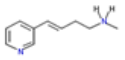	TI-6[d]	10000	ND
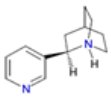	TI-3_R[d]	41	384		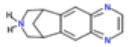	Varenicline[d]	ND	ND

[a]Taken from [18] Talley, T.; Yalda, S.; Ho, K.; Tor, Y.; Soti, F.; Kem, W.; Taylor, P., Spectroscopic analysis of benzylidene anabaseine complexes with acetylcholine binding proteins as models for ligand-nicotinic receptor interactions. *Biochemistry* **2006**, *45* (29), 8894-902.

[b] Taken from [2, 4] Celie, P.; van Rossum-Fikkert, S.; van Dijk, W.; Brejc, K.; Smit, A.; Sixma, T., Nicotine and carbamylcholine binding to nicotinic acetylcholine receptors as studied in AChBP crystal structures. *Neuron* **2004,** *41* (6), 907-14.

[c] Taken from [2, 19] Taylor, P.; Talley, T.; Radic', Z.; Hansen, S.; Hibbs, R.; Shi, J., Structure-guided drug design: conferring selectivity among neuronal nicotinic receptor and acetylcholine-binding protein subtypes. *Biochem Pharmacol* **2007,** *74* (8), 1164-71.

[d] Private communication from Dr. Todd T. Talley, UCSD.

Using the crystallographic coordinates as starting points, each co-crystal structure ligand was protonated and then minimized to the local minimum conformation using the Jaguar default settings (Schrodinger, Inc). Each minimized ligand was then docked into the Nic,[4] Cce,[4] Apo,[5] Epi,[5] Mla,[5] and Lob AChBP[5] crystal structure (with and without) a water of crystallization. Docking into the various L and A-AChBP protein structures (after removal of bound ligand) for proteins without water of crystalliztion was carried out using CDOCKER and Glide (4.5). A minimum of 10 poses were saved for each ligand. An RMSD value for each saved pose was then calculated by comparison to the original co-crystal structure ligand pose. This provides a measure of the ability of the program to reproduce the experimental pose in the LBD. To assess the ability of each program's scoring function to accurately rank order various poses compared to the experimental pose for each ligand, the score vs. the RMSD were plotted and correlation coefficients (R^2) were calculated using Microsoft Excel.[17]

Low energy conformations for each ligand were also docked into various AChBPs, but with an explicit water to provide the possibility for water-mediated hydrogen bonding between the putative hydrogen-bond acceptor of each ligand, and the backbone of the protein in the LBD. These studies were only carried out using CDOCKER and Glide v 4.5. A minimum of 20 poses were saved and the RMSD was again calculated for each pose referenced to the crystal structure pose. The water molecule chosen was the one that mediates the hydrogen bond from the nicotine pyridine ring to Met 114 in the Lymnaea crystal structure. All the other AChBPs were superimposed with the Nic AChBP by sequence alignment and the water molecule from the Nic AChBP was copied to the other AChBPs.

For all docking studies, the binding site residues and the water molecule were selected to generate the grid and the sphere for docking the compounds with Glide v 4.5 and CDOCKER. Glide docking studies were carried out at both Standard and Extra Precision levels.

A second set of docking experiments were performed with 19 NNR ligands (represented as individual compounds, diasteriomers based on variation in protonation of tertiary amines or differing starting conformations) using the Standard Precision algorithm available from Glide v 5.0. Several of these ligands were those co-crystallized with either *Lymnaea stagnalis* or *Aplysia californica* AChBP). Low energy conformations for all ligands (as the protonated species where appropriate) were generated using either Sibyl (Tripos, Inc.), Mopac AM1 or Jaguar (Schrodinger, Inc.).

Ligands were docked into protein structures representing both species (A-apo[5], A-hepes,[20] A-epi,[5] A-lob,[5] L-hepes[13] and L-nic[4]) where the co-crystal ligand had been removed. For each docking study, a maximum of 20 poses was saved for each ligand. Using a perl script developed for this purpose, each asset of poses was analyzed (Pipeline Pilot, Accelrys, Inc.) via a protocol that ranked the poses for each ligand, based on similarity to known geometric parameters derived under Aim 1. Pharmacophoric distances and angles were measured for each pose for all ligands, using the same metrics as those measured in the ligand-protein geometrical analyses. Poses were sorted based on cation-π distance and indole N to I118 or M114 amide N depending on if the protein, i.e., from aplysia or lymnaea, respectively. RMSD values were calculated for each ligand when co-crystal structures were available. The protein was frozen in every docking study, with only the ligand allowed to move.

Aim 3. Scoring Functions

Where binding data were available, the Glide scoring function and the scoring functions implemented in CDOCKER were used to investigate the correlation between scoring function and Kd binding affinity values to L-AChBP and A-AChBP for each of these NNR ligands. The Score Ligand Poses protocol available from Accelrys Discovery Studio 2.1 was also utilized to score poses for ligands docked into each AChBP from both sets of docking jobs. Correlation between the best scoring pose for each ligand and the pK_d (-log(Kd)) was calculated for each protein-ligand docking set.

CHAPTER IV

RESULTS

AChBP Geometrical Analysis

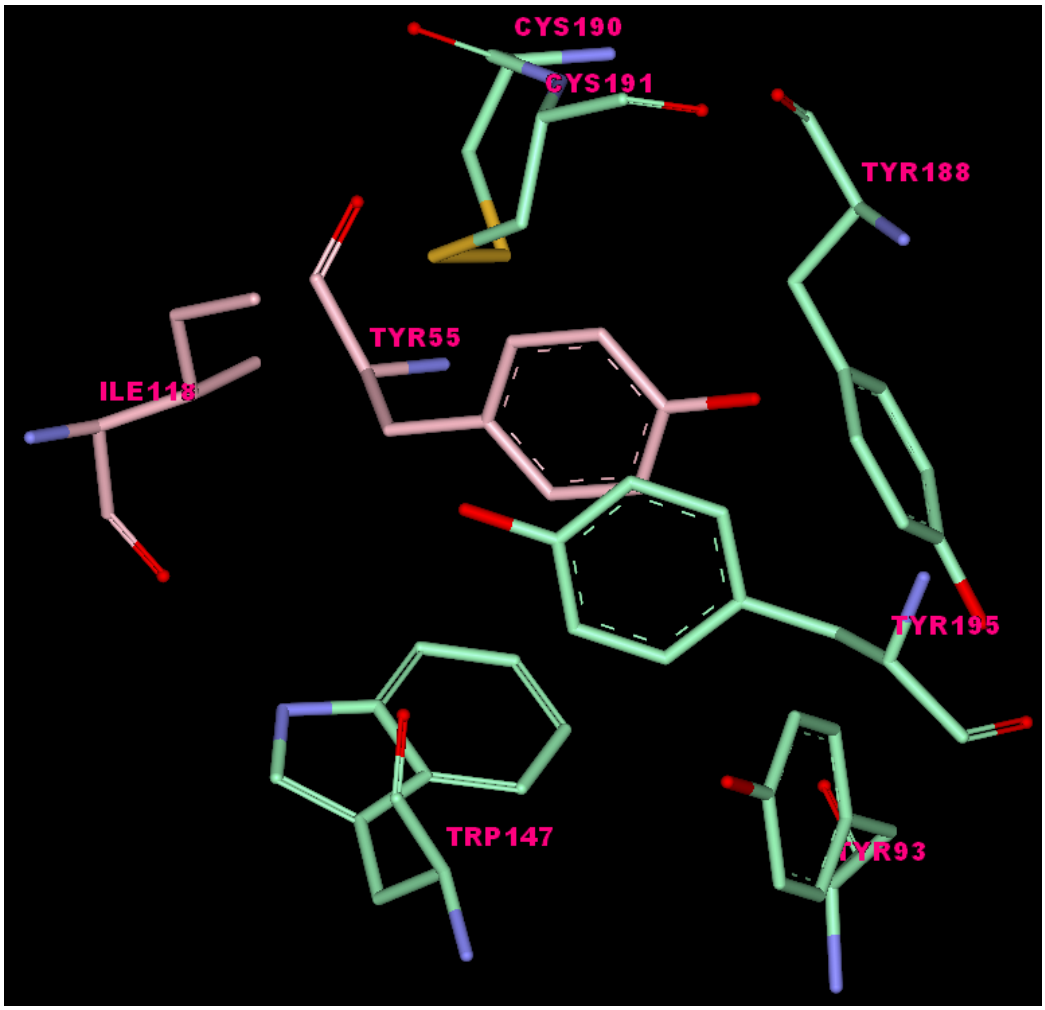

Figure 8. Ligand binding domain residues.

Figure 8 shows key residues in the LBD for which pharmacophoric distances and angles were measured. Figure 9 summarizes results for both intra and inter-protein structure comparisons of various distances in co-crystal LBDs. For example, Fig 9a shows the average distance (and standard deviation) between W147 and the centroid defined by the ring (defined from the α carbon to the sulfur for each cysteine residue) for C190-C191for the occupied and unoccupied LBDs. Measures were taken and compared for the co-crystal structures for IMI-,[5] EPI-,[5] MLA-,[5] HEPES-,[20] LOB-A-AChBP[5] as well as the average distances and standard deviation for NIC- and CCh-L-AChBP,[4] and CAPS-B-AChBP.[14] In all cases, distances are relative to the APO-A-AChBP.[5]

As noted by Hansen, residues on the C-Loop (C190, C191, Y188 and Y195) move closer to W147 compared to the apo[5] structure for the smaller ligands, and stay in similar positions (MLA) or move further away for the largest ligand, i.e., IMI, see Figs. 9a, 9b and 9e. Further, the distance between the two residues Y195 on the principal face and Y55 on the complementary face differ with each ligand, (Fig 9f) indicating a breathing motion for the side-to-side dimensions of the LBD. This analysis, however, shows a greater level of detail than has been provided previously. For example, one notes that the distance given by the W147-to-C190, 191 centroids shows relatively little variation within a protein from one LBD to another, and similar average differences from one co-crystal structure to another for all of the small ligands, even cross species, i.e., A- to L- to B-AChBP. Further, ligand binding in all cases cause a small expansion of the relative distance from W147 (principal face) to Y55 (or W55) on the complimentary face (Fig 9c). Also, it should be noted that movements of the C-loop, brought on by binding, are asymmetrical, with Y195 moving towards W147 to a much lesser extent (about 2 Å, see fig 9e) compared to the much larger movement of Y188 (Fig. 9b). As noted by

Hansen, lobeline stands out compared to the other small ligands in that binding causes an opening of the side-to-side distance as evidenced by the expansion of the W147 to Y93 distance, compared to contraction of that distance in all other small ligands (and even large ligand cases, see Fig 9d).

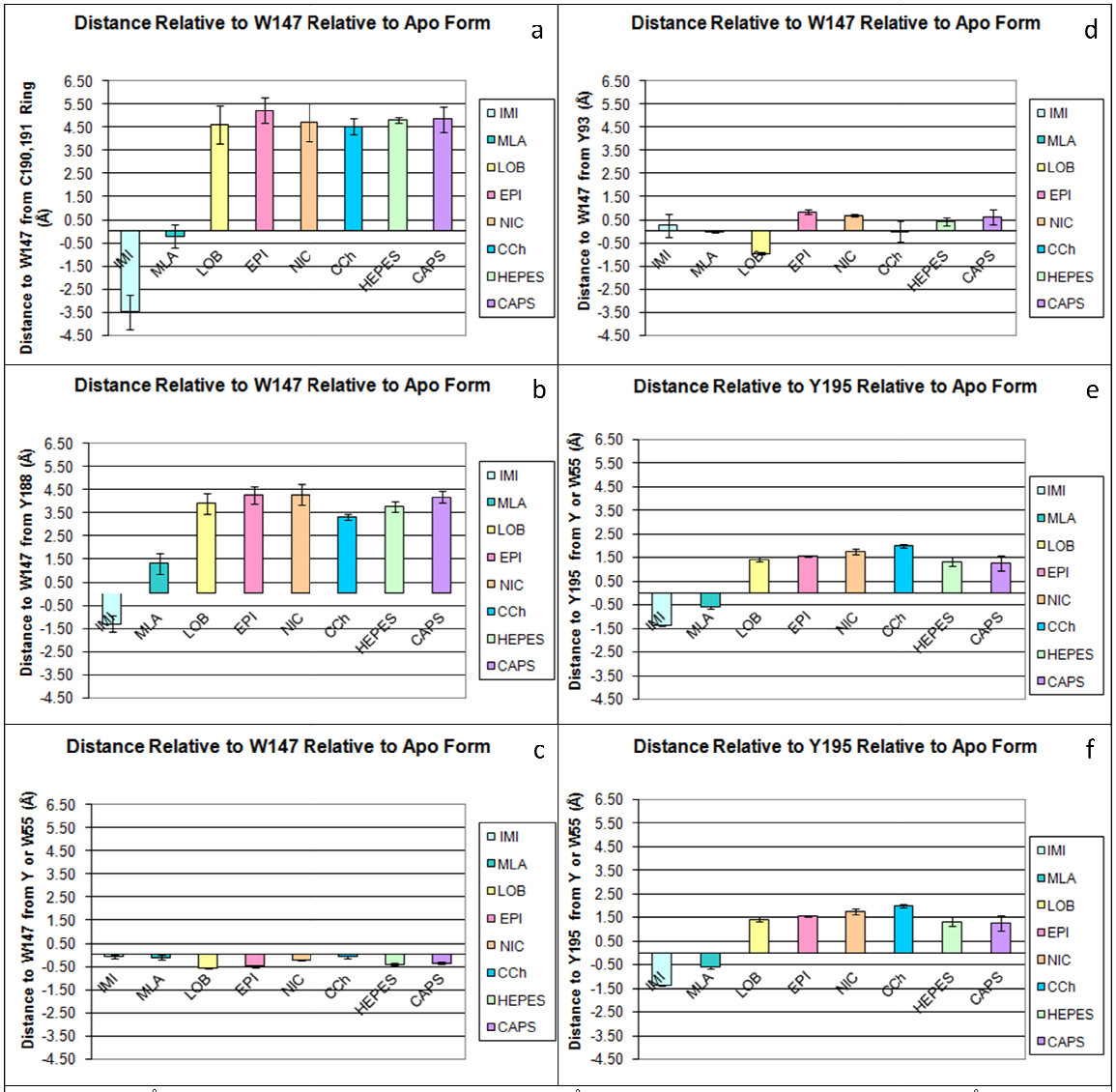

Figure 9. Binding Site Distances Measured. All distances are relative to the Apo form. See Appendix A, Figure 25, for definitions of measured distances.

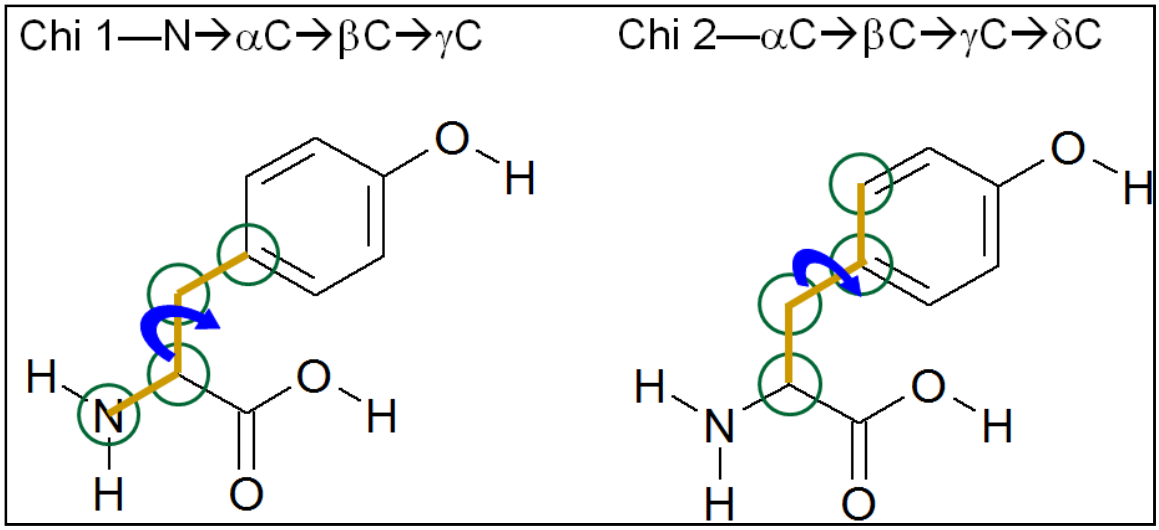

Figure 10. Definition of Chi1 and Chi2 angles.

Fig 10 shows atoms used to define the Chi1 and Chi2 angles. Fig 11 demonstrates that Chi1 varies little compared to the Apo[5] form for all co-crystal structures analyzed with two exceptions. Y55, which varies with each ligand since this residue comes from the complementary face; and, Y93, which is close to trans for lobeline where this residue has moved out of the way to provide additional space for one of lobeline's phenyl groups.

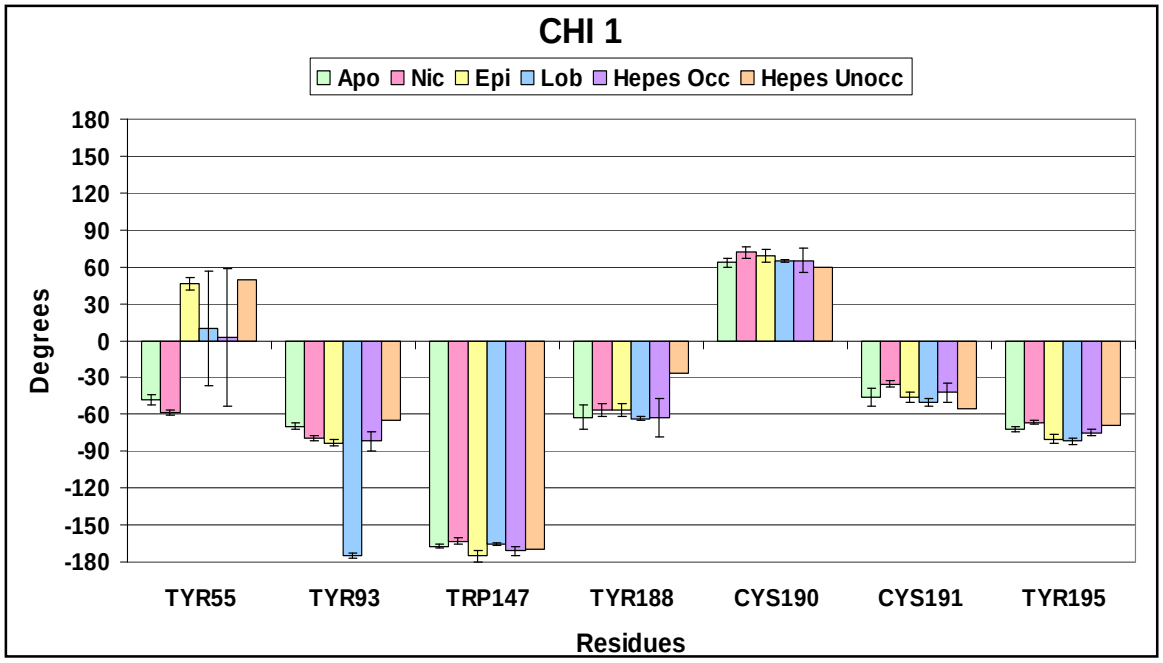

Figure 11. Chi 1 Angles. Chi 1 angles as defined in Fig. 10; angles are not relative to the Apo form.

As indicated by Figure 12, Chi2 tends to vary for each ligand such that the protein adjustes to accommodate the ligand. Further, one may note that in the case of the 5 LBDs for the HEPES structure, there is relatively little change for the occupied LBDs Hepes Occ) compared to those that are unoccupied (Hepes Unocc) by this weakly bound ligand. The standard deviations calculated for the distances, chi1 and chi2 angles of the proteins indicate that all the binding sites are indeed structurally similar with few exceptions (hepes and lob).

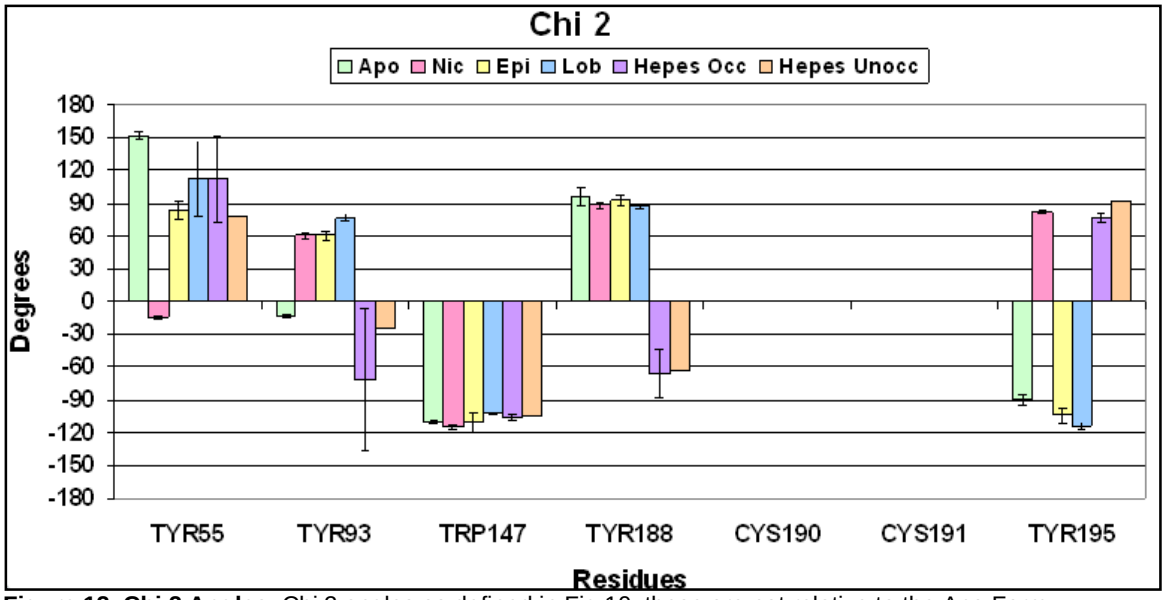

Figure 12. Chi 2 Angles. Chi 2 angles as defined in Fig 10; these are not relative to the Apo Form.

Figure 13 shows that distances from the ligand cationic center to the aromatic residue centroids of the LBD vary by as little as 1 Å to as much as 3 Å for all ligands analyzed. The torsions and angles vary by 20 to 50 degrees from the smallest to the largest angles for all of the ligands analyzed (Figure 14). These data will provide useful guidelines to sort out poses for each ligand during docking studies. Only those poses that fall within the normal distance and angle ranges will be analyzed.

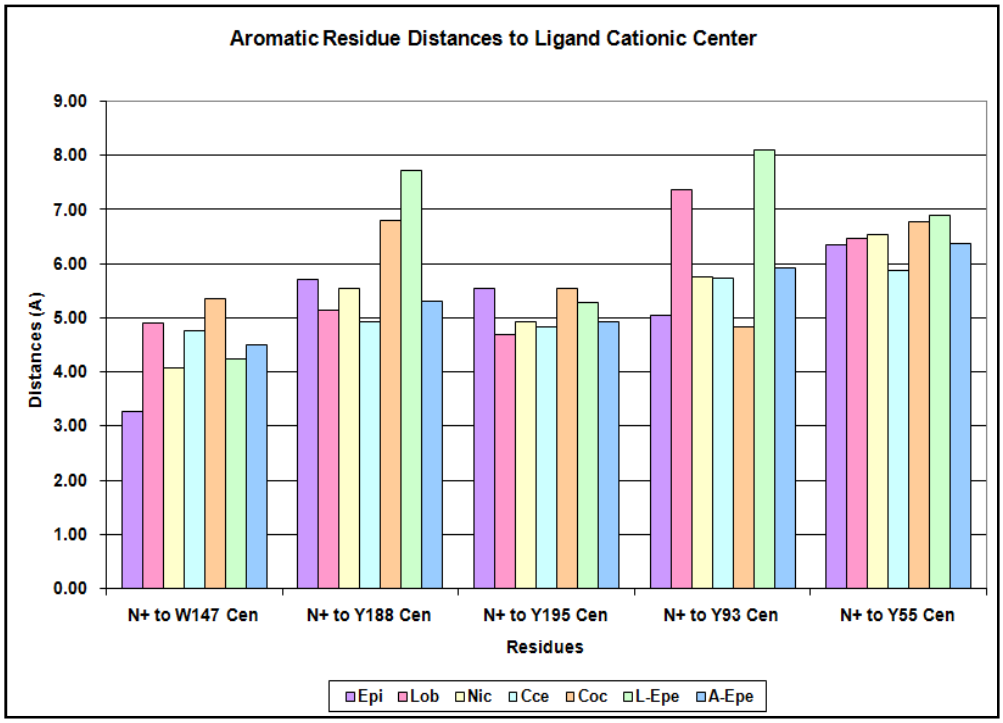

Figure 13. Distances from the Ligand Cationic Center to Binding Site Residues. Distances from the ligands cationic center to the centroid of the aromatic residues in the LBD. Measured for Epi, Lob, Nic, Cce, Coc, L-hepes (L-EPE) and A-hepes (A-Epe).

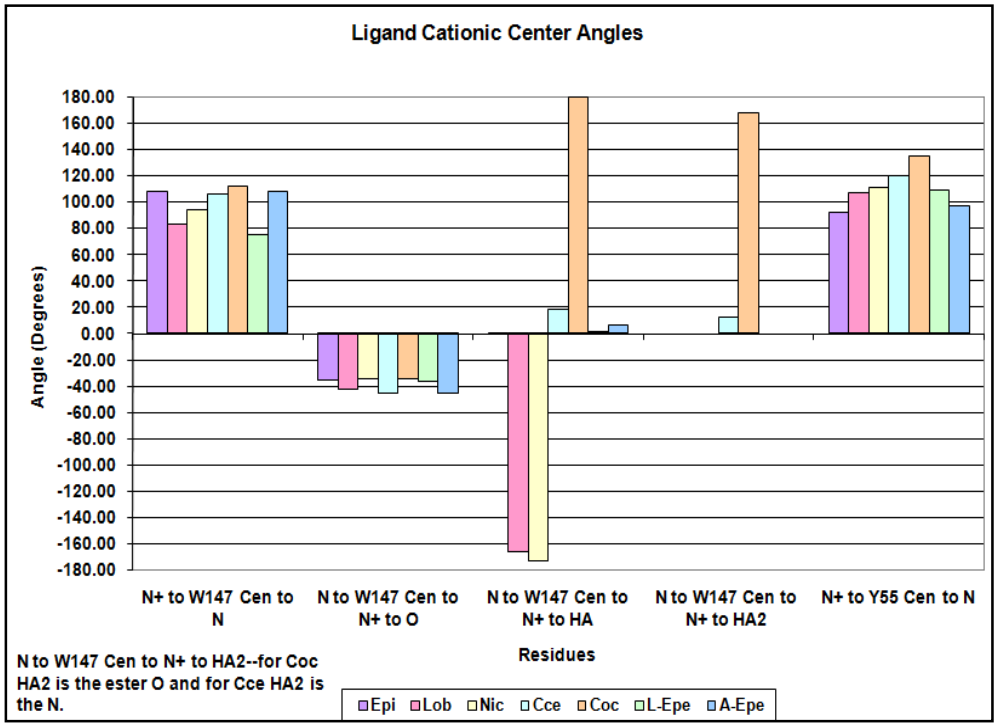

Figure 14. Angles from the Ligand Cationic Center to Binding Site Residues Angles and torsions measured for Epi, Lob, Nic, Cce, Coc, L-hepes (L-EPE) and A-hepes (A-Epe).

Table 2 provides a detailed ligand-protein analysis for distances, angles and torsion angles for each of the five LBDs for the EPI-A-AChBP and NIC-L-AChBP co-crystal structures. Torsion angles, plane angles and distances were measured using the cationic center of each bound ligand to the aromatic residues for each binding site of the epibatidine and nicotine co-crystal structures. Distances from the cationic nitrogen to the centroid for W147, as well as the cationic nitrogen and the centroid for Y93 are significantly different for the epibatidine co-crystal structures when compared to the nicotine co-crystal structures at the $p = 0.05$ level, indicating a closer movement of the epibatidine ligands to the aromatic residues compared to that for nicotine. This is of interest since epibatidine binds with substantially higher affinity at both A- and L-AChBP, indicating that epibatidine is utilizing more efficiently LBD interactions than does nicotine. The cationic center to Y188, cationic center to Y195 and the cationic center to Y55 distances are all equivalent in all the LBDs across these two proteins.

Additional distance and angle measurements were taken for the distance from W147 indole N to I118 amide N and the angle from W147 indole N to I118 carbonyl O to I118 carbonyl C. These measurements were taken to assess the relative movement of the two subunits which form the LBD. These data, for torsions, angles, and distances measured for one ligand binding domain from each co-crystal structure, suggest that the protein undergoes a conformational change upon ligand binding and the changes are specific to the shape and size of the ligands.

Table 2. W147 to I118 Measurements. Distance, angle and Torsion angle measurements for all 5 different LBDs for nic and epi co-crystal structures. N^+—Cationic Center, Cen—ring centroid, N—W indole ring, O—W carbonyl O, and HA—hydrogen bond acceptor.

	W147/143	Y188/185	Y195/192	Y93/89	Y55/W52	W147/143	W147/143	W147/143	Y55/W53
	N+ to W147 Cen	N+ to Y188 Cen	N+ to Y195 Cen	N+ to Y93 Cen	N+ to Y55 Cen	N+ to W147 Cen to N	N to W147 Cen to N+ to O	N to W147 Cen to N+ to HA	N+ to Y55 Cen to N
Ligand	Distance	Distance	Distance	Distance	Distance	Angle	Torsion Angle	Torsion Angle	Angle
epi (AE)	3.27	5.71	5.55	5.04	6.35	108.00	-34.98	-0.17	92.39
epi (ED)	3.19	5.48	5.96	5.11	5.62	107.70	-43.66	8.47	94.79
epi (DC)	3.77	5.50	5.51	4.87	6.12	115.50	-34.53	1.81	91.49
epi (CB)	3.73	5.20	5.20	4.84	6.36	109.00	-31.35	-2.62	101.67
epi (BA)*	4.11	5.36	4.50	5.06	7.13	96.50	-27.86	-1.04	102.68
nic (AB)	4.07	5.54	4.92	5.76	6.54	94.20	-34.27	-172.99	111.51
nic (BC)	4.42	5.08	4.49	5.87	6.80	96.10	-31.45	177.21	111.56
nic (CD)	4.14	5.49	4.84	5.76	6.46	95.40	-35.01	-176.11	112.38
nic (DE)	4.30	5.43	4.66	5.95	6.67	96.50	-32.67	-173.47	112.10
nic (EA)	4.21	5.37	4.62	5.86	6.34	99.50	-35.20	-177.34	110.81
W is numbered 147 in the Aplysia AChBP and is 143 in Lymnaea AChBP									
*structure w/ pyridine ring rotated 180°									

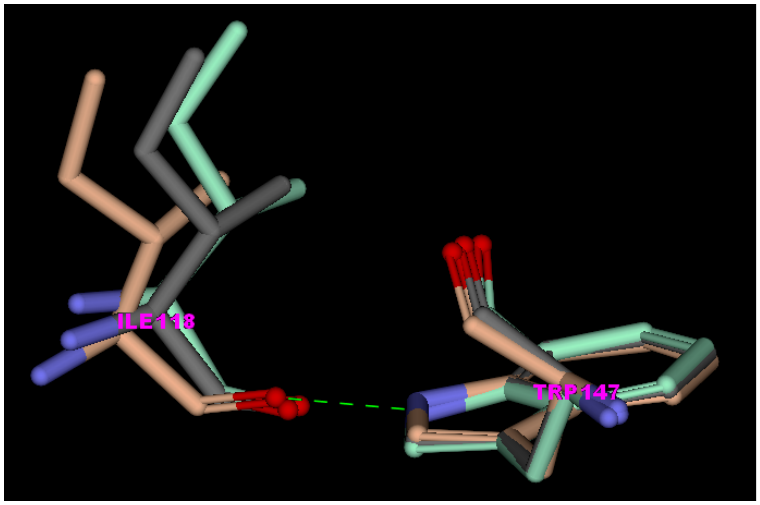

Figure 15. Complementary Face Changes Relative to the Principal Face. Apo, lobeline and epibatdine structure superimposed on W147. Shows the movement in I118 from the complementary face suggesting that the complementary face adjusts to the ligand. Pink—lobeline, Green—epibatidine, and Gray—Apo.

The distance measurements indicate that the two subunits that make up the binding domain in the Aplysia-lobeline co-crystal structure move further apart from each other when compared to the apo and epibatidine structures,[5] Figures 16, 17a and 17b. (Lobeline binding seems to push the two subunits apart). In addition to the subunits moving apart, lateral movements of the two subunits with respect to each other were also observed. W147 to I118 carbonyl O to I118 carbonyl C illustrated that the epibatidine structure had the greatest angle. This large angle indicates that the α-C has shifted laterally but the hydrogen bonding interaction between the indole N-H of W147 and the carbonyl O of I118 kept carbonyl O of the residue in place and moved the rest of the residue, which causes the I118 carbonyl group in the epibatidine structure to form an angle such that, when overlapped the carbonyl bond of the epibatidine structure intersects with the carbonyl bond of the apo form. However, the lobeline structure I118 carbonyl group only intersects with the apo form at the carbonyl O.

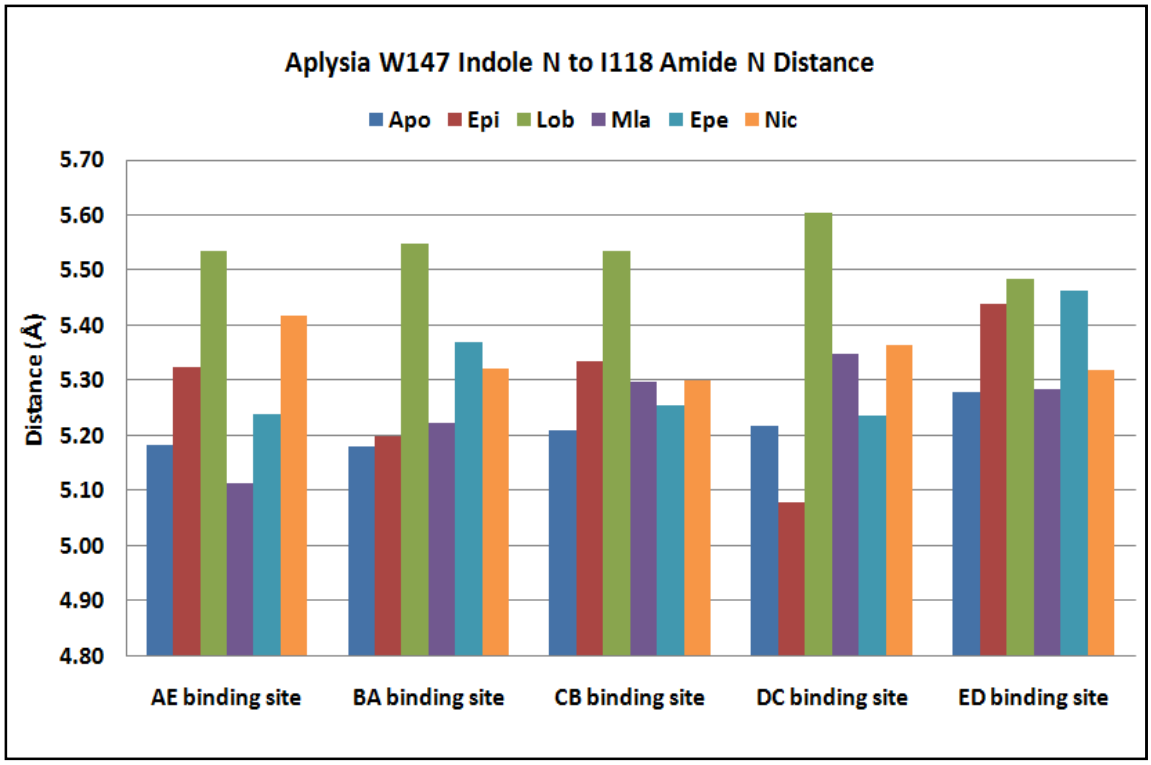

Figure 16. Distances Between the Prinicpal and Complementary Faces. All of the distances measured were co-crystallized with Aplysia, except for nicotine, which was crystallized in Lymnaea.

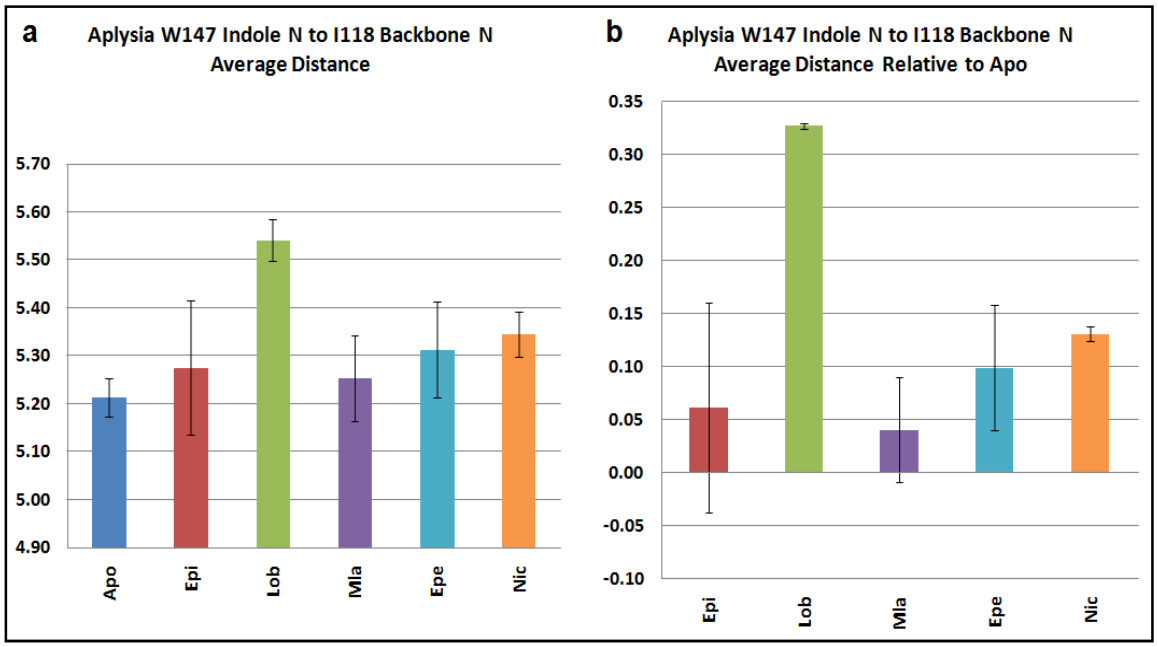

Figure 17. Distances Between the Prinicpal and Complementary Faces Averaged. Part a shows the average distances between W147 indole nitrogen and I118 amide nitrogen with error bars. Part b shows the averages relative to the apo form with error bars.

AChBP Docking Studies

Docking Analysis with crystal structure ligands

Docking Without Water

Docking studies were carried out on all ligands where published co-crystal structures with either A- or L-AChBP are available. As noted previously, attempts were made to reproduce representative crystal structure poses, both in the presence and absence of a molecule of water, present in many co-crystal structures in the HBA region of the ligands. Docking analysis without the water of crystallization indicated that the epibatidine crystal structure pose was reproduced when docked into in most of the AChBPs except for the MLA structure, using CDOCKER or Glide SP and XP. However, the lobeline and imidacloprid crystal structure poses were only reproduced in the lobeline AChBP. As for nicotine, the crystal structure pose was only reproduced in the lob, epi, and nic AChBPs using all the methods tested. Glide SP and XP docking algorithms were able to reproduce the crystal structure pose for nicotine in the cce,[4]and apo[5] structure as shown by the RMSD. Interestingly none of the docking algorithms reproduced the crystal structure poses for any of the ligands in the MLA AChBP. Unfortunately, there was no correlation with any of the scoring function scores and the root mean square deviation (RMSD) of the poses to the crystal structure pose.

Table 3. Crystal Structure Ligands Docked Without Explicit Water. Lowest RMSD (Å) for the poses docked without water of crystallization using Glide (SP and XP) and CDOCKER, compared to the co-crystal structure for that same ligand.

Docked Without Water						
		Ligands RMSD				
Protein	Method	Epibatidine	Lobeline	Nicotine	Imidacloprid	Average
CCE	Glide SP	0.65	-----	1.05	-----	0.85
	Glide XP	0.61	-----	1.10	-----	0.86
	CDOCKER	0.62	4.52	1.57	1.36	2.02
NIC	Glide SP	1.23	-----	0.37	2.17	1.26
	Glide XP	1.50	-----	0.40	2.37	1.42
	CDOCKER	0.68	5.21	0.29	0.96	1.79
APO	Glide SP	0.89	2.97	1.75	7.62	3.31
	Glide XP	0.62	2.79	1.56	5.85	2.71
	CDOCKER	2.67	5.36	2.20	3.73	3.49
EPI	Glide SP	1.33	-----	0.96	1.88	1.39
	Glide XP	0.48	-----	0.74	1.86	1.03
	CDOCKER	0.56	5.66	0.80	1.29	2.08
MLA	Glide SP	6.57	2.65	1.53	6.57	4.33
	Glide XP	6.61	3.14	5.01	6.28	5.26
	CDOCKER	3.66	3.28	2.60	2.19	2.93
LOB	Glide SP	0.62	0.94	1.64	1.70	1.23
	Glide XP	1.13	1.09	1.75	2.83	1.70
	CDOCKER	0.77	1.01	0.90	3.35	1.51

Docking With Water of Crystalliztion

Docking the low energy crystal structure ligands with inclusion of a molecule of water (taken from the nicotine co-crystal structure in the HBA region) helped to improve the reproducibility of the crystal structure poses for most of the ligands except for lobeline. For example, epibatidine and nicotine crystal structure poses were reproduced in most of the AChBPs tested using CDOCKER and Glide SP and XP, except in a few cases. On the other hand, the lobeline crystal structure pose was only found when

docking occurred into the lobeline crystal structure, for all three docking methods. As for imidacloprid, the explicit water did help the docking methods reproduce the crystal structure pose in more of the AChBPs. In conclusion, while a water of crystallization does improve the accuracy of the docking algorithms, scoring functions still do not correlate well with the RMSD values. There did appear to be a trend towards better correlation of the Glide GScore to experimentally determined Kd values than that found for the CDOCKER score, but the data set is too small to judge. RMSDs to prove how close the docked pose is to the crystal structure are needed here.

Table 4. Crystal Structure Ligands Docked With Explicit Water. Lowest RMSD (Å) for the poses docked with water of crystallization using Glide (SP and XP) and CDOCKER.

Docked With Water						
		Ligands RMSD				
Protein	Method	Epibatidine	Lobeline	Nicotine	Imidacloprid	Average
CCE	Glide SP	0.55	-----	1.19	-----	0.87
	Glide XP	0.38	-----	1.14	-----	0.76
	CDOCKER	0.60	4.38	1.24	1.30	1.88
NIC	Glide SP	0.69	-----	0.38	1.98	1.02
	Glide XP	0.61	-----	0.41	2.02	1.01
	CDOCKER	0.99	4.70	0.37	0.79	1.71
APO	Glide SP	1.09	2.66	1.08	7.90	3.18
	Glide XP	1.81	2.55	7.40	7.60	4.84
	CDOCKER	0.80	3.14	1.93	0.77	1.66
EPI	Glide SP	1.34	-----	1.06	1.90	1.43
	Glide XP	1.34	-----	0.42	1.92	1.23
	CDOCKER	0.52	6.60	0.58	1.13	2.21
MLA	Glide SP	6.75	3.62	7.54	2.54	5.11
	Glide XP	0.46	3.15	7.41	6.28	4.33
	CDOCKER	1.36	3.11	1.65	0.71	1.71
LOB	Glide SP	1.25	1.44	2.61	1.77	1.77
	Glide XP	1.17	0.89	1.70	2.74	1.63
	CDOCKER	0.52	0.80	0.70	1.51	0.88

Docking Analysis with 19 NNR ligands.

Docking studies were carried out on a diverse set of 19 NNR ligands for which Kd data are available, docked with a water of crystallization. Analysis of the resulting docked poses and docking scores indicated that an H-bond term for water-ligand HBA was not reflected in the score. Careful observation of the poses with the explicit water molecule showed that the orientation of the hydrogen atoms on the explicit water molecule were rotated so that it no longer held the conformation that would let it

hydrogen bond to the ligand and I118 or M114 depending on the crystal structure species used. Therefore, all of the data for the docking studies with water will be excluded from the following discussions. Data for the docking studies without water were analyzed and are presented in Figures 16 to 20.

It is of note that careful analysis of the lobeline and nicotine co-crystal structures shows that the explicit water in the lobeline structure was shifted closer to I118 than it was to M114 in the nicotine structure. An explanation for this observation is that the lobeline structure is wider than the nicotine structure, so when lobeline binds, the hydrogen bond acceptor ends up closer to I118 and, pushes the explicit water molecule closer to I118. Thus, we now have good evidence for the importance of a water in the HBA region, and the likelihood that the water adjusts for each ligand.to optimize the hydrogen bond donor-hydrogen bond acceptor interaction.

As a result of the docking studies without water, the AChBP structures that have been co-crystallized with smaller ligands, such as the nicotine, epibatidine, aplysia hepes and lymnaea hepes, have a tighter ligand binding domain than the lobeline and apo[5] AChBP structures. Therefore, the limitation in using a docking tool that keeps the protein frozen is that bulkier ligands such as lobeline and DMXBA cannot fit into the ligand binding domain of one of the tighter AChBP structures. So, the Nic, Epi, A-Epe, and L-Epe structures were analyzed only for the ligands that were docked into the binding site.

Based on our earlier geometrical analyses, Glide 5.0 was able to find the “expected pose” for each ligand that was docked. However, the “expected pose” was not always the best scored pose. Therefore the “expected pose” was determined by: (1)

using the range of 3-5.5 Å for the distance between the cationic center and the centroid of the indole ring on W147. This served as a filter to eliminate poses in which the cationic center is too far away from the indole ring of W147 to from the expected cation-π interaction; (2) using the range of 3.5 to 6.5 Å for the distance between the hydrogen bond acceptor on the ligand and the indole ring N on W147. This served to filter out poses with the hydrogen bond acceptor in a region that was very different from that observed in known crystal structures; and (3) using the crystal structures as guides, the poses that were not eliminated, were carefully observed for the orientation of the cationic center and the hydrogen bond acceptor in order to identify that orientation closest to the crystal structures. In the case where more than one pose appeared to be the "expected pose", the pose with the lowest (more negative) Gscore was selected as the "expected pose".

Since the K_d data were obtained from different labs and by different techniques, variations in K_d values can be expected. The K_d values that were obtained in Palmer Taylor's lab at UCSD were determined by measuring the displacement of tritiated epibatidine by the ligand being tested. However, some of the data from the Taylor 2007 review article[19] were taken from other sources. The K_d values for epibatidine, lobeline, methyllycaconitine and α-conotoxin[5] were determined using the ratio of dissociation to association rates by monitoring intrinsic tryptophan quenching with stopped flow spectrofluorometry. In order to simplify the data for graphing, K_d values were converted to the pK_d (pKd = log(1/Kd)). A higher pK_d value indicates that the ligand shows higher binding affinity.

The glide scoring function, called the Gscore,[21] assigns the poses a score based on the interaction energies between the posed ligand and the protein. The equation Schrodinger released for the Gscore is as follows:

$$Gscore = a* vdW + b * Coul + Lipo + Hbond + Metal + Rewards + RotB + Site$$

- a = 0.050, b = 0.150 for Glide 5.0
- vdW = van der Waals interaction energy
- Coul = Coulomb interaction energy
- Lipo = Lipophilic-contact plus phobic-attractive term
- HBond = Hydrogen-bonding term
- Metal = Metal-binding term (usually a reward)
- Rewards = Various reward or penalty terms
- RotB = Penalty for freezing rotatable bonds
- Site = Polar interactions in the active site
- (GScore = 10000.0 indicates that a given ligand pose failed one or more criteria for computing GScore. Depending on which ones it failed, the components of GScore may not be valid either.)

The more negative Gscore reflect better interaction between the ligand and the protein. However, as revealed below, the best Gscore was not assigned to the compound with the highest pK_d. It is possibly that this occurs because the Gscore equation does not have a term for the cation-π interaction, an interaction believed to drive ligand binding in the NNRs.

Based on the information that poses assigned a more negative Gscore have a better score and the larger the pK_d value imply better binding affinity, if a correlation exists between the Gscore and the pK_d, the trend line (in a plot of Gscore vs. pK_d) should have a negative slope. The negative slope implies that ligands with lower binding affinity (poorer pK_d values) should be assigned a more positive Gscore and ligands with higher binding affinity (more positive pK_d values) should get a more negative Gscore. In the results discussed below, the degree of correlation of these two quantities was

evaluated using the R^2 value resulting from a linear least squares fit of the data. Docking experiments that yielded a higher R^2 were deemed the better results. An R^2 value of about 0.8 is expected for the docking study.[17] In general, all of the correlations observed between the Gscore and the pK_d were very low. As discussed below, in comparisons of the data from each AChBP structure the lobeline AChBP structure was found to have a better correlation between the pK_d and the Gscore than other AChBP structures studied.

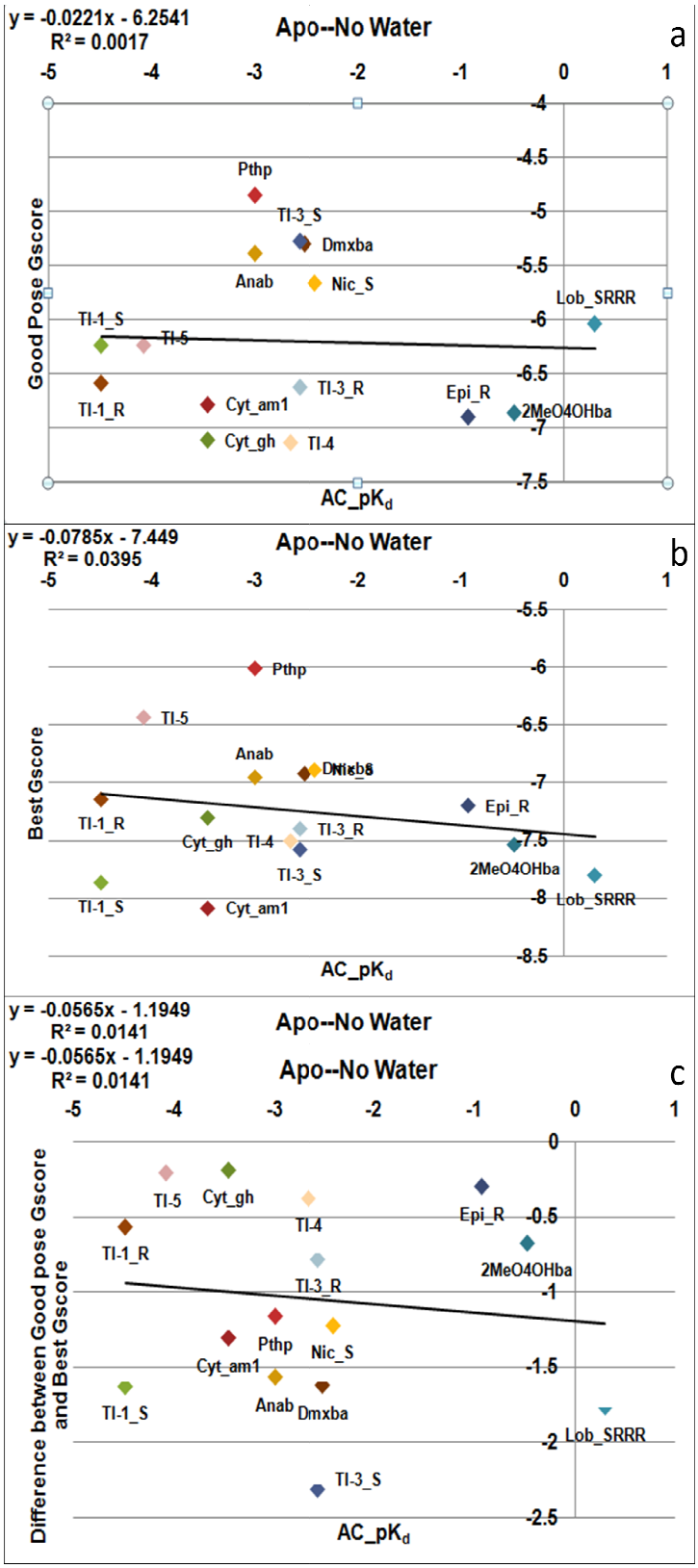

Figure 18. Docking Results for Ac-Apo Without Explicit Water. The data shows the correlation between the Gscore and pK_d. Part a shows the correlation between the Gscore for the expected pose for each ligand docked. Part b shows the best Gscore versus the pK_d, while Part c) shows the graph of the difference between the best Gscore and the expected pose Gscore versus the pK_d. The pK_d values were calculated by taking the log of ($1/K_d$) with the K_d expressed in nanomolar units.

DOCKING STUDIES: Aplysia Apo[5] AChBP Structure

Glide 5.0 managed to dock 14 out of the 19 ligands from the dataset (see Table 1) into the aplysia apo[5] AChBP structure. Figure 18a illustrates a plot of the "expected pose" Gscore vs. the pK_d. No correlation was observed because the data is too scattered, the R^2 = 0.002. Figure 18b shows the best Gscore and the pK_d. No correlation was observed here either (R^2 = 0.040). After no

correlation was observed in Figures 18a and b, the difference between the best Gscore and the “expected pose” Gscore was graphed (Figure 18c). No correlation was observed from this graph as well (R^2 = 0.010). The C-Loop conformation in the Apo[5] form may affect the correlation as it does not optimize interactions with the ligands. Therefore the Apo structure may not be the best template from which to construct a homology model useful for docking NNR ligands.

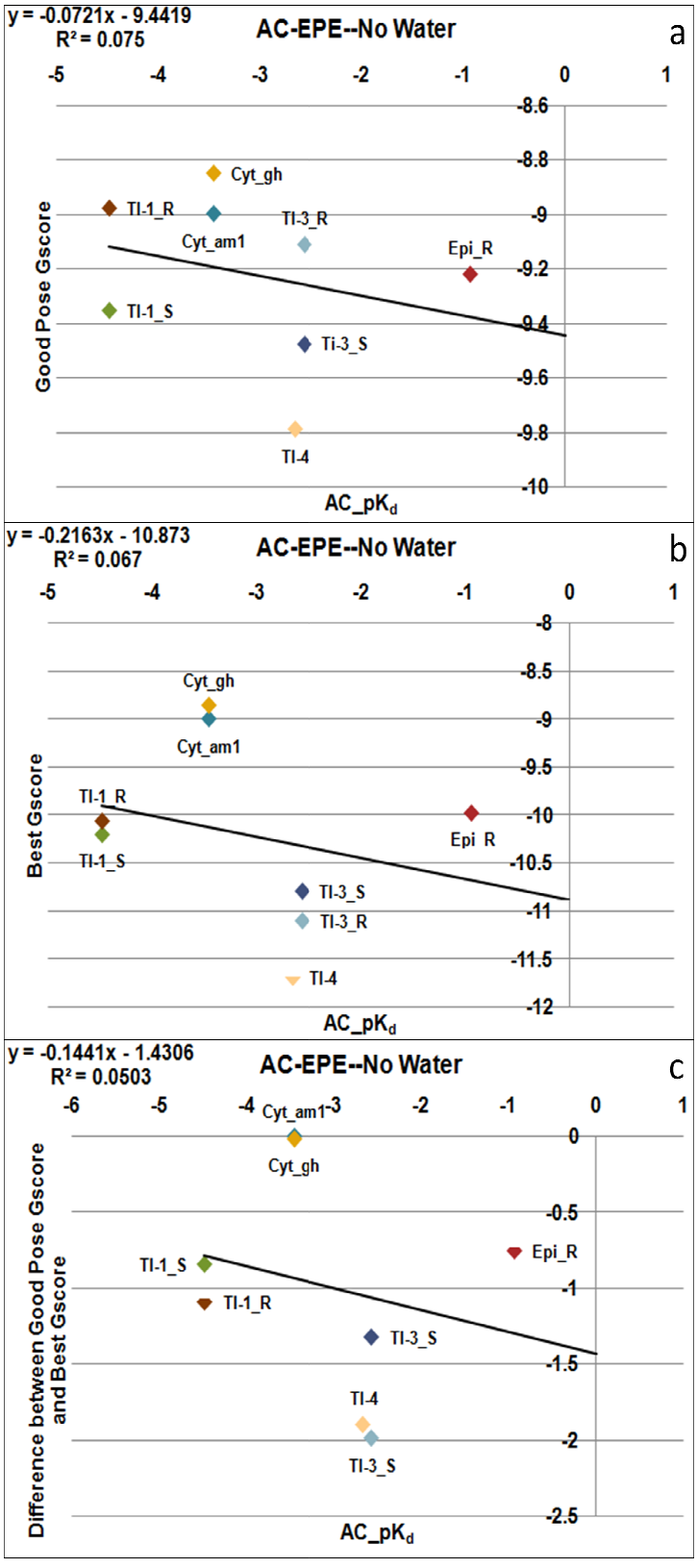

Figure 19. Docking Results for Ac-Epe Without Explicit Water. The data shows the correlation between the Gscore and pK_d. a) shows the correlation between the Gscore for the expected pose for each ligand docked. b) shows the best Gscore versus the pK_d, and c) shows the graph of the difference between the best Gscore and the expected pose Gscore versus the pK_d. The pK_d values were calculated by taking the log of ($1/K_d$) with the K_d expressed in nanomolar units.

DOCKING STUDIES: Aplysia Hepes AChBP Structure

The aplysia hepes structure was more difficult to dock ligands into. Glide 5.0 was able to dock only 7 of the 19 ligands from the dataset. The "expected pose" Gscore vs. the pK_d is plotted in Figure 19a. The correlation coefficient for Figure 19a (R^2 = 0.075) showed a slight improvement but was still very low. The slope of the trend line of the aplysia hepes graph (figure 19a) is more negative

than the slope of the trend line from the aplysia apo[5] graph (figure 18a) implying that the Aplysia hepes structure may be a slightly better template for a NNR homology model. Figure 19b shows the graph of the best pose Gscore vs. the pK_d. Again, correlation for docking into aplysia hepes (Figure 19b) seems to be slightly better when compared to that for docking to the apo structure (Figure 18b). Again, the trend line has a slightly more negative slope than that found for aplysia apo[5]. Figure 19c demonstrates a scatter plot of the difference between the "expected pose" Gscore and the best pose Gscore vs. pK_d. Comparing figure 19c to figure 18c, one can conclude that the trend line in figure 19c actually has a more negative slope than that of figure 18c. While docking to the aplysia hepes AChBP structure displays a slightly higher correlation between the Gscore and pK_d values, Glide 5.0 was only able to dock 7 out of the 19 NNR ligands into this structure, so while better than the aplysia Apo structure, it is still not a very good template.

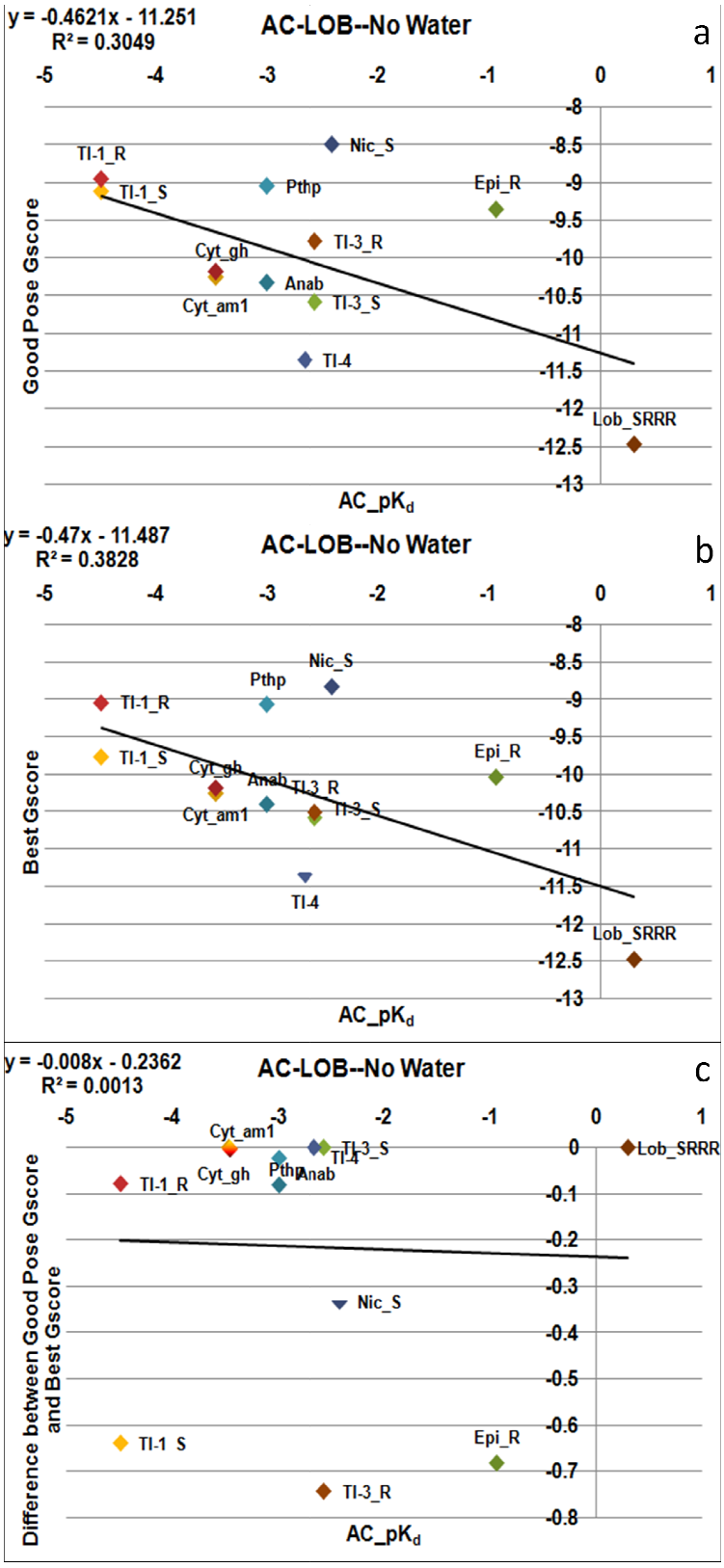

Figure 20. Docking Results for Ac-Lob Without Explicit Water. The data shows the correlation between the Gscore and pK_d. Part a shows the correlation between the Gscore for the expected pose for each ligand docked. b) Shows the best Gscore versus the pK_d, and c) shows the graph of the difference between the best Gscore and the expected pose Gscore versus the pK_d. The pK_d values were calculated by taking the log of ($1/K_d$) with the K_d expressed in nanomolar units.

DOCKING STUDIES:

Aplysia Lobeline AChBP Structure

Glide 5.0 was able to dock 10 out of the 19 NNR ligands into the aplysia lobeline structure. A small correlation was observed between pK_d and both the "expected pose" Gscore (Figure 20a) and the best Gscore (figure 20b). R^2 values are 0.305 and 0.383 respectively. Figure 20c illustrates a scatter plot of

the difference between the “expected pose” Gscore and the best pose Gscore vs. pK_d. Figure 20c shows that the varience in the error (predicted vs actual) between these two measures is essentially evenly distributed. Comparison of figures 18a, 18b, 19a, 19b, 20a and 20b suggests that the lobeline AChBP structure (figures 20a and 20b) would be the best template for NNR homology modeling because these graphs show the best correlation between the pK_d and the Gscore and these graphs have a trend line with the most negative slope. The conclusion drawn from this data is that the lobeline structure is the best template for NNR homology modeling.

However, the data in figure 20a and 20b may be skewed by the lobeline point, which falls in the lower right hand corner of the graph, while the rest of the data is clustered together in the middle of the graph. The possibility exists that the correlation observed in figures 20a and 20b could be a “pseudo-correlation.” Glide 5.0 assigned the lobeline point the best (most negative) score and lobeline had the best (highest) pK_d of all the ligands docked into the lobeline AChBP crystal structure. A reason for the lobeline point having the best score could be that the protein was optimized for lobeline, since it was co-crystallized with lobeline. Therefore, the lobeline point in figures 20a and 20b seems to be driving the correlation, so it was removed in order to determine whether the correlation actually exists or not.

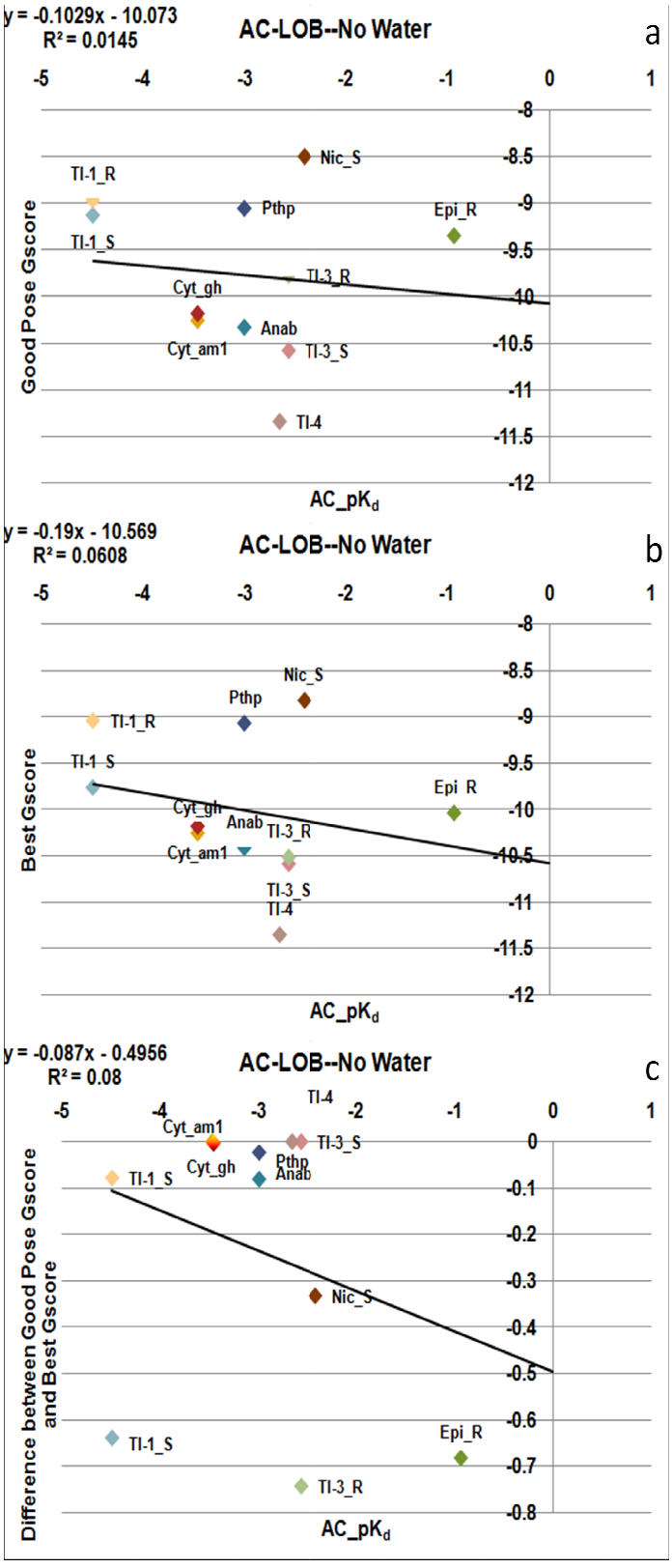

Figure 21. Docking Results for Ac-Lob Without Explicit Water—Lobeline Point Removed. This point was removed because the data was skewed. The data shows the correlation between the Gscore and pK_d. Part a shows the correlation between the Gscore for the expected pose for each ligand docked. b) shows the best Gscore versus the pK_d, and c) shows the graph of the difference between the best Gscore and the expected pose Gscore versus the pK_d. The pK_d values were calculated by taking the log of ($1/K_d$) with the K_d expressed in nanomolar units.

<u>DOCKING STUDIES: Results for Ac-Lob without water with the lobeline point removed.</u>

After removal of the lobeline point from the graphs (figure 20a, b and c) the correlation between the expected pose Gscore and the pK_d disappeared, figure 21a. The new R^2 value is 0.0145. However, the trend line still has a negative slope. Removal of the lobeline point tremendously reduced the correlation between the best Gscore and the pK_d

figure 21b. R^2 for the skewed data was 0.383 and R^2 for the data with the lobeline point removed is 0.061. Although the correlation was reduced for the “expected pose” Gscore and the best Gscore, it was increased for the graph of the difference between the “expected pose” Gscore and the best Gscore vs. pK_d. The R^2 value before the point was removed was 0.0013, and the R^2 value after removal of the lobeline point was 0.08. Nevertheless, comparing the lobeline graphs that were not skewed (figure 21a, b and c) to the aplysia hepes graphs (figure 19a, b and c), the conclusion remains that the lobeline AChBP structure would be the best template for an NNR homology model.

Careful comparison of the R^2 value for the “expected pose” Gscore vs. pK_d for the aplysia hepes (figure 19a) structure was 0.075, which suggests a better correlation for the hepes structure than that present in the lobeline data that was not skewed (figure 21a) which has an R^2 value of 0.0145 suggests that the hepes structure would be the better template for NNR homology modeling. Also the R^2 value from the hepes best pose Gscore vs. pK_d graph (figure 19b) was 0.067 and lobeline structure graph of best pose Gscore vs. pK_d that was not skewed had an R^2 value of 0.061. These data also suggest that the hepes structure would be the best template for NNR homology modeling. The R^2 values of figures 19c and 21c are 0.0503 and 0.08 respectively. In this case the data suggests that the lobeline structure would be the best template for NNR homology modeling. Although the most of the data suggests that the hepes structure has a better correlation with the Gscore, the lobeline structure would still be the best template for NNR homology modeling because Glide 5.0 docked more of the ligands into this structure than in the hepes structure.

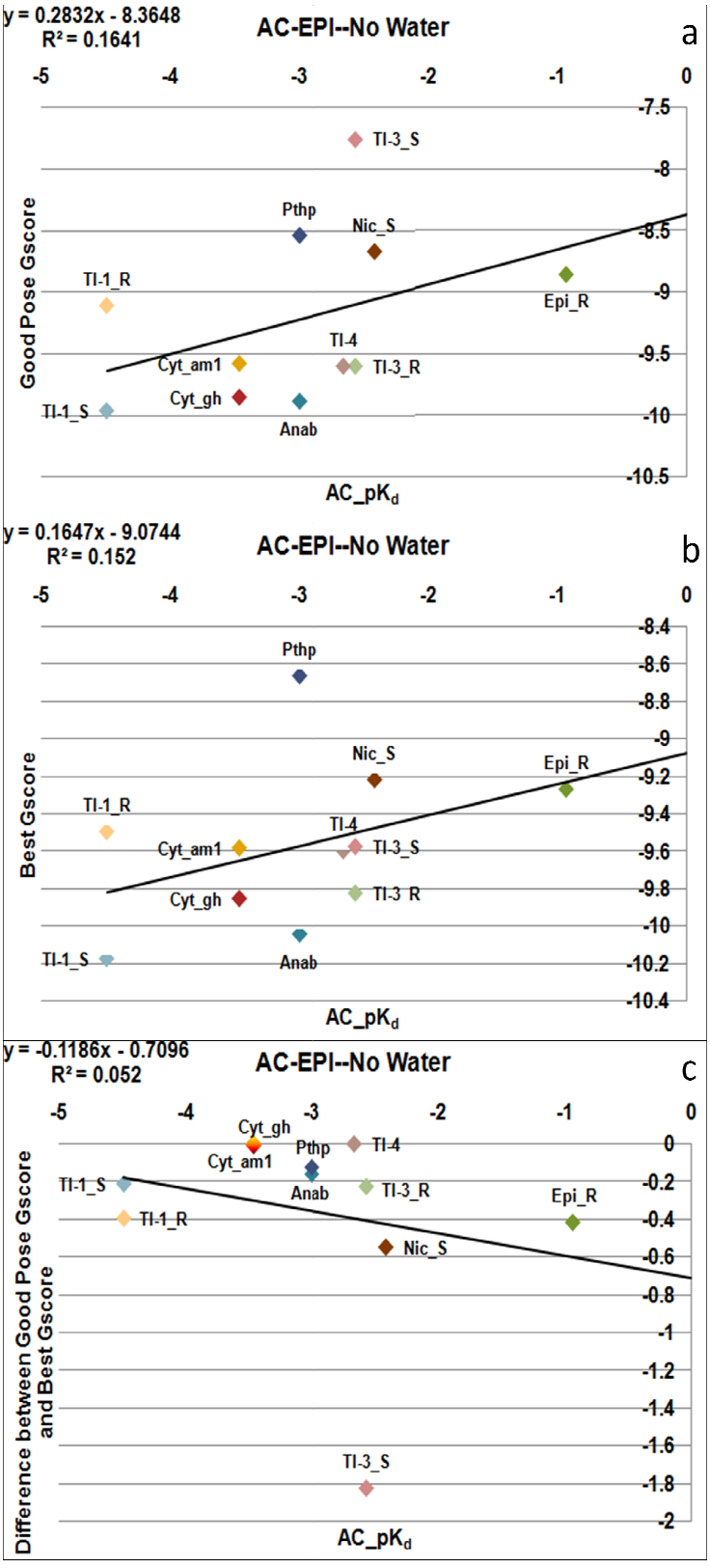

Figure 22. Docking Results for Ac-Epi Without Explicit Water. The data shows the correlation between the Gscore and pK_d. Part a shows the correlation between the Gscore for the expected pose for each ligand docked. b) shows the best Gscore versus the pK_d, and c) shows the graph of the difference between the best Gscore and the expected pose Gscore versus the pK_d. The pK_d values were calculated by taking the log of ($1/K_d$) with the K_d expressed in nanomolar units.

DOCKING STUDIES: Aplysia Epibatidine Structure

The aplysia epibatidine structure had some major problems. Glide 5.0 was able to dock only 9 out of the 19 ligands into the epibatidine ligand binding domain. The correlation observed from the graph of the "expected pose" Gscore vs. the pK_d (figure 22a) was not very good, the R^2 value was 0.1641. Also the correlation observed from the graph of the best pose

Gscore vs, pK_d (figure 22b) was similar to that observed in figure 22a. The R^2 value was 0.152. The slope of the trend line for figures 22a and b is positive which implies that the ligands with better binding affinity were assigned a more positive score and the ligands with worse binding affinity were assigned a more negative score, opposite to the expected trend. Figure 22c shows a graph of the difference between the "expected pose" Gscore and the best pose Gscore vs. the pK_d. The trend line from figure 22c does have a negative slope, which indicates that the largest change in the Gscore occurred for the ligands with better binding affinity. The data shown in figure 22c has an R^2 value of 0.0052, which indicates that the correlation between the Gscore and the pK_d for the aplysia epibatidine structure is non-existent. Based on these low correlations, the inverted trend and the low number of ligands that successfully dock, it appears that epibatidine may not be the best starting point for most NNR homology models.

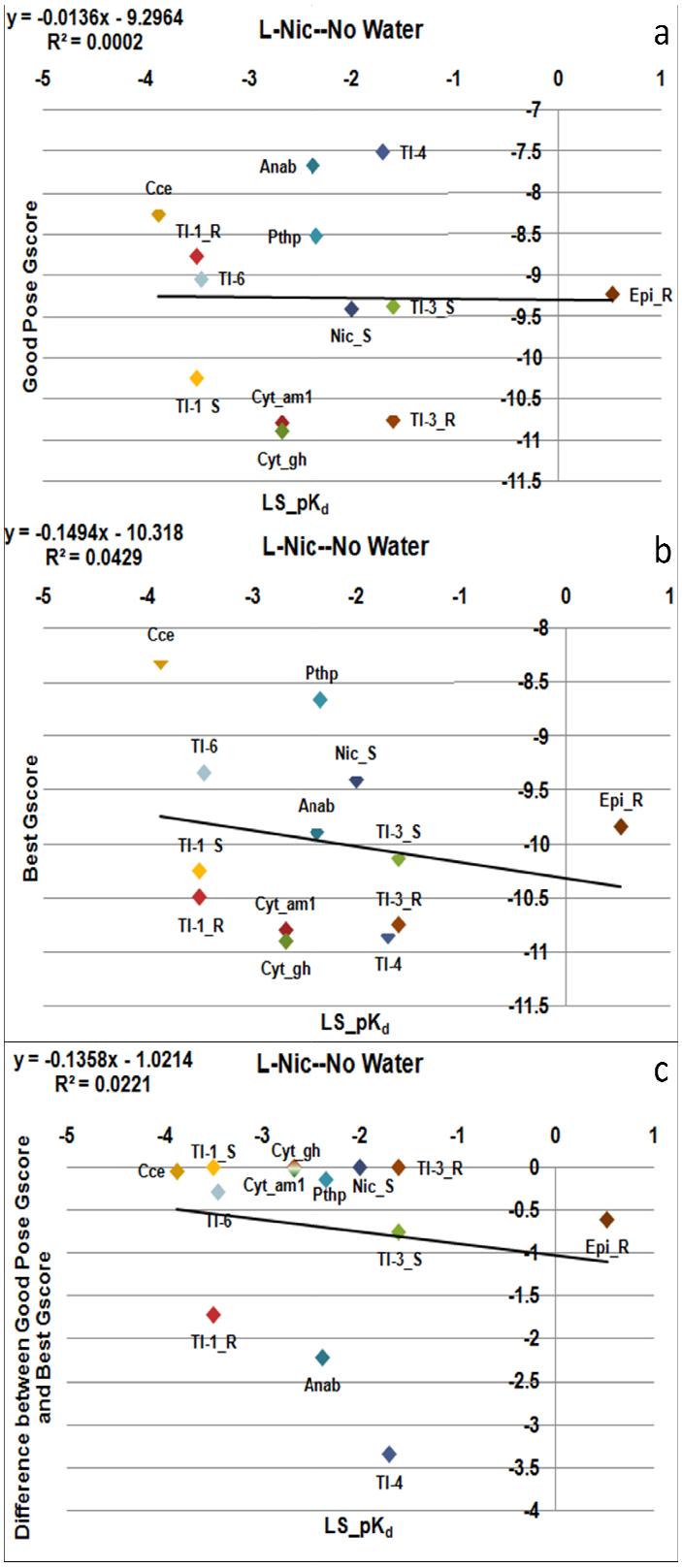

Figure 23. Docking Results for Ls-Nic Without Explicit Water. The data shows that the correlation between the Gscore and pK_d. Part a shows the correlation between the Gscore for the expected pose for each ligand docked. b) shows the best Gscore versus the pK_d, and c) shows the graph of the difference between the best Gscore and the expected pose Gscore versus the pK_d. The pK_d values were calculated by taking the log of ($1/K_d$) with the K_d expressed in nanomolar units.

DOCKING STUDIES: Lymnaea Nicotine Structure

Glide 5.0 was able to dock 12 of the 19 ligands from the data set into the nicotine structure. No correlation was observed between the "expected pose" Gscore and the pK_d (figure 23a). The trend line has a negative slope and the correlation coefficient was 0.0002, which is worse than the correlation of the lobeline structure that was not skewed. Figure 23b shows a graph of the best Gscore vs. the pK_d. The

trend line has a negative slope and the R^2 value from this graph is 0.0429, which is also less than that of the lobeline structure where the data was not skewed by the lobeline point (R^2 = 0.061). Finally, figure 23c shows a graph of the difference between the "expected pose" Gscore and the best Gscore vs. the pK_d. The trend line has a negative slope and the R^2 value for this graph was 0.0221, which was also less than that of the lobeline structure that was not skewed (R^2 value was 0.08). These data suggest that the lobeline AChBP structure may be the best starting point for NNR homology modeling.

Interestingly, the shape of the nicotine binding site and the epibatidine binding site are very similar, since both ligands have a similar shape. However, nicotine was co-crystallized with the *Lymnaea* species, which has a tryptophan in the place of tyrosine 55 in the *Aplysia* structures. The trend lines from the epibatidine AChBP structure studies has a positive slope and the trend lines from the nicotine AChBP studies has a negative slope. The difference in the slopes of the trend lines could be due the lower resolution of the epibatidine structure, since the other aplysia structures (such as apo, hepes and lobeline) all had trend lines with a negative slope. Since nicotine and epibatidine are similar in shape, the nicotine AChBP crystal structure would not be a good template for building a homology model into which bulkier ligands would be docked into. However, if one wanted to dock NNR ligands similar to nicotine and epibatidine in shape and size then the nicotine AChBP structure would be a good model.

Although, Glide 5.0 was able to dock more of the ligands into the nicotine AChBP structure, the R^2 values were still less than that of ligands docked into the lobeline structure with the lobeline point removed. Since the data was scattered, no matter which

structure was used, the next step would be to look for a correlation between other scoring functions and the pK_d.

Scoring Functions

Since the Ac-Lobeline structure seemed to have the most promising correlation, other scoring function analyses were examined to determine if these might improve correlations between experimental data and the predicted binding score. Other scoring function analyses were also carried out on the Ls-Hepes (L-Epe) structure because it was the most open structure available from the *Lymnaea stagnalis* species.

The scoring functions available from Discovery Studio 2.1 package (LigScore 1 and 2, PLP 1 and 2, Jain, PMF and PMF4, and Ludi); assign positive scores to the more favorable interactions. Therefore, the ligands with higher binding affinity should be assigned a more positive score, unlike the Gscore, where ligands with higher binding affinity should have been assigned a more negative score. Upon observation of the relationship between the pK_d and the other scoring functions, no scoring function was identified that had a positive slope and a good R^2 value.

To better account for key cation-π interactions in the LBD, the Quantum Mechanical Polarized Ligand Docking (QPLD) protocol from Schrodinger was examined. Table 5 indicates that of all the scoring functions studied for the lobeline AChBP, the QPLD Gscore was the best because the trend line had a negative slope and it had the best correlation with the pK_d ($R^2 = 0.42$).

Table 5. A-Lob Other Scoring Functions. Best Score from Different scoring functions for Structures Docked into the Lobeline AChBP.

Best Score from Different Scoring function for Structures Docked into the Lobeline AChBP														
Name	Ac_K_d_nM	AC_pK_d	LigScore1_Dreiding	LigScore2_Dreiding	-PLP1	-PLP2	Jain	-PMF	-PMF4	Ludi_1	Ludi_2	Ludi_3	QPLD G_score	QPLD G_energy (CvdW)
lobelinesrrrh_gh	0.5	0.30	2.75	4.93	120.16	124.42	8.56	148.01	93.22	608	533	951	-12.81	-58.92
TI-4H_GH	460	-2.66	2.45	4.27	82.18	78.88	5.61	140.33	94.17	480	421	675	-11.65	-36.52
lobelinersssh_gh_5	0.5	0.30	2.83	5.52	126.51	120.3	7.84	160.53	93.61	657	561	815	-12.21	-52.73
TI-3H_GH	370	-2.57	2.21	4.27	80.06	78.61	5.95	129.83	88.94	441	389	644	-10.78	-34.92
TI-3H_up_GH	370	-2.57	2.11	4.3	75.45	71.76	5.7	125.73	90.82	410	371	628	-10.82	-35.62
anabaseine	1001	-3.00	2.74	4.6	73.92	69.26	3.47	117.45	79.99	445	367	844	-10.03	-35.54
cytisineh_am1	2926	-3.47	2.43	4.22	70.88	63.39	5.23	121.97	77.16	392	363	913	-10.30	-31.10
cytisineh_gh	2926	-3.47	2.54	4.31	72.56	65.28	5.6	123.54	76.14	416	387	888	-10.20	-30.89
epirh-6311ss-blyp	8.6	-0.93	2.63	4.83	78.46	78.55	4.62	124.55	85.86	464	392	647	-9.99	-39.23
TI-1rsH_GH	31000	-4.49	2.57	4.7	73.25	69.94	4.79	108.79	89.81	385	363	612	-9.84	-33.79
pthp_h	1001	-3.00	2.55	4.89	71.87	66.64	3.36	94.53	80.86	416	329	868	-8.83	-30.92
TI-1srh_gh	31000	-4.49	2.69	4.4	75.91	72.83	4.81	114	89.61	401	370	639	-9.68	-34.76
TI-5H_GH	12000	-4.08	3.42	5.92	119.43	111.34	4.44	151.92	107.47	671	508	833	-9.19	-49.34
nicotine_rsth_mmff	260	-2.41	2.25	4.37	66.48	64.41	3.66	102.92	78.44	394	361	608	-9.56	-33.31
nicotine_ssch_mmff	260	-2.41	1.56	4.28	63.54	61.28	4.22	113.15	85.74	345	334	579	-8.40	-32.82
dmxba_h	330	-2.52	0.81	2.62	91.52	89.71	6.06	134.42	79.94	673	542	1183		
2meo4ohba_h	3	-0.48	1.08	2.95	98.69	97.47	5.63	133.6	78.58	599	482	1110		
Correlation			**-0.20**	**-0.04**	**0.55**	**0.61**	**0.62**	**0.50**	**-0.007**	**0.49**	**0.56**	**0.29**	**-0.64**	**-0.65**
R2			**0.04**	**0.00**	**0.30**	**0.38**	**0.38**	**0.25**	**0.00**	**0.24**	**0.31**	**0.08**	**0.42**	**0.43**
Slope			**-0.09**	**-0.02**	**7.28**	**8.40**	**0.59**	**5.96**	**-0.04**	**36.94**	**29.07**	**35.68**	**-0.53**	**-3.79**

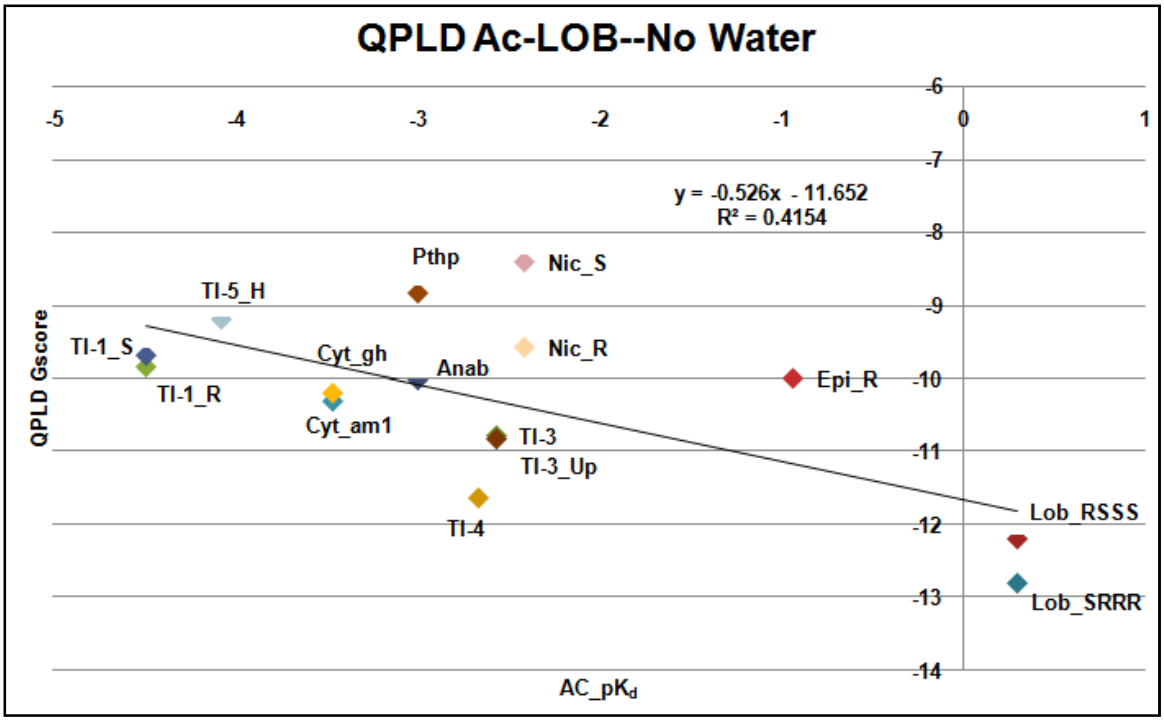

Figure 24. QPLD Gscore vs. pK_d Graph.

Table 6 indicates that none of the other scoring functions, including the QPLD Gscore, has a good correlation with the pK_d for the Lymnaea hepes structure. Lack of correlation between the scoring functions and the pK_d may be due to the difference in the species, in which a tyrosine in aplysia has been replaced by a tryptophan in lymnaea. Since tryptophan is bulkier than tyrosine, the tryptophan contributes to the tightness of the ligand binding domain. Therefore, there would not be as much room in the hepes structure as there is in the lobeline structure for the ligand to interact favorably.

Table 6. L-Hepes Other Scoring Functions. Best Score from Different Scoring function for Structures Docked into the L-Hepes AChBP

Best Score from Different Scoring function for Structures Docked into the L-Hepes AChBP														
Name	Ls_K_d_nM	LS_pK_d	LigScore1_Dreiding	LigScore2_Dreiding	-PLP1	-PLP2	Jain	-PMF	-PMF4	Ludi_1	Ludi_2	Ludi_3	QPLD G_score	QPLD G_energy (CvdW)
lobelinersssh_gh_16	130	-2.11	2.74	4.75	97.05	103.73	7.25	177.99	119.69	571	499	737	-11.54	-42.56
lobelinesrrrh_gh_10	130	-2.11	2.79	4.85	102.05	104.56	5.88	179.98	115.22	577	522	795	-11.65	-40.59
TI-4H_GH_4	50	-1.70	2.35	4.55	78.92	79.17	5.36	163.43	115.52	432	391	694	-10.47	-37.10
TI-3H_GH_19	40	-1.60	1.96	4.49	68.96	69.17	4.72	148.71	103.87	406	361	665	-10.03	-32.65
TI-1srh_gh_10	3200	-3.51	2.27	4.11	64.2	60.99	3.97	129.13	107.21	379	357	672	-10.26	-30.88
TI-1rsH_GH_14	3200	-3.51	1.74	4.03	61.77	64.31	2.74	124.8	103.28	342	331	644	-9.49	-30.40
TI-3H_up_GH_6	40	-1.60	1.96	4.62	69.54	70.9	3.87	143.44	105.12	370	356	667	-10.23	-35.05
cytisineh_gh_5	480	-2.68	3.18	4.59	59.34	60.85	4.39	145.83	94	415	372	807	-8.90	-32.31
epirh-6311ss-blyp_6	0.3	0.52	2.77	4.88	69.34	71.42	3.71	140.15	107.13	449	365	632	-8.84	-37.43
nicotine_ssch_mmff_4	100	-2.00	2.03	4.1	63.26	64.7	4.03	122.5	96.5	404	369	628	-9.89	-32.21
anabaseine_3	240	-2.38	2.3	4.6	58.74	59.57	3.02	127.83	91.44	399	345	844	-8.70	-30.40
nicotine_rsth_mmff_19	100	-2.00	1.66	3.92	58.65	60.6	2.85	124.69	96.92	337	331	636	-8.91	-30.12
cytisineh_am1_5	480	-2.68	2.84	4.47	58.7	62.15	5.01	140.73	91.84	381	374	819	-9.61	-32.84
TI-5H_GH_4	1000	-3.00	3.21	5.06	90.17	92.71	4.47	181.98	122.29	550	444	952	-9.30	-43.02
hepes_zwit_mmff_7	265	-2.42	3.17	4.35	67.85	69.96	3.59	121.39	91.21	242	287	274	-9.39	-30.86
TI-6H_RS3_GH00019_9	2900	-3.46	2.69	4.32	63.12	63.87	3.89	126.85	92.63	395	356	618	-8.17	-34.04
carbamylcholine_9	7575	-3.88	2.45	4.12	47.8	41.57	1.5	59.16	54.69	257	258	250	-8.71	-35.21
pthp_h_11	220	-2.34	2.06	4.8	58.67	64.41	3.9	80.69	73.15	371	304	806	-7.12	-28.23
2meo4ohba_h_1	0.43	0.37	2.13	4.21	78.94	79.1	5.77	164.06	101.9	600	503	904		
dmxba_h_3	19	-1.28	2.43	4.4	80.39	81.8	5.73	110.38	67.71	635	538	856		
R			**-0.11**	**0.24**	**0.32**	**0.34**	**0.41**	**0.33**	**0.21**	**0.48**	**0.43**	**0.29**	**-0.14**	**-0.20**
R^2			**0.01**	**0.06**	**0.10**	**0.11**	**0.17**	**0.11**	**0.05**	**0.23**	**0.18**	**0.09**	**0.02**	**0.04**
Slope			**-0.05**	**0.07**	**3.96**	**4.50**	**0.47**	**8.87**	**3.17**	**45.68**	**29.35**	**45.68**	**-0.16**	**-0.85**

Possible Causes for Data Scatter

Variability introduced by obtaining K_d values from different labs and by different experimental protocols could be a reason for the scatter of the data. In addition, the fact that the scoring functions do not have a term for cation-π interactions, which is believed to drive ligand binding to the AChBPs and NNRs, could also contribute for the scatter in the data. Another reason could be that the proteins are flexible and they reorient amino acid side chains to accommodate the ligand, however in the docking studies reported here the protein is frozen and only the ligand is allowed to move. Therefore, the interactions between the ligand and protein that would contribute to large pK_d may not be observed in docking studies, where the protein is frozen and favorable interactions may be missed because the protein was not allowed to adjust to the ligand.

CHAPTER V

CONCLUSION

General Conclusion

The AChBP ligand binding domain is located on the outside midsection of the protein and is at the interface of two of the five subunits that make up these homopentamers. The C-Loop, located on the principal face, closes over the binding pocket when an agonist binds. Contrastingly, upon binding of a peptide antagonist, like α-connotoxin, the C-Loop moves further away from the position of the C-Loop in the apo AChBP. As observed from the binding of an agonist and a peptide antagonist, the geometry of the AChBP ligand binding domain changes with ligand binding. Some of these changes are due to the C-loop moving to close over the top of the binding site allowing an agonist ligand to interact with the two tyrosines (Y188 and Y195) that are on both sides of the C-loop and forming a portion of the aromatic box in the LBD. Further, both subunits move relative to each other upon ligand binding. The C-loop for the lobeline structure is in roughly the same position as that found for the other small agonists ,i.e., epibatidine and nicotine, but residues are arranged differently to make room for the more extended structure of lobeline, leaving the binding pocket more open than the co-crystal structures of epibatidine or nicotine. Finally, as evidence of the repositioning of the two subunits with binding, the two subunits that make up the ligand binding domain for the lobeline structure are further apart from each other than any of the other structures.

Docking of crystal structure ligands into proteins derived from the co-crystal structures of epibatidine, nicotine, lobeline and imidaclopride structures (with and without an explicit water), was most promising for the lobeline structure, providing the best average RMSD for the four ligands docked. The second set of docking studies also suggests the lobeline AChBP should be the best template for homology modeling, with Glide 5.0 successfully docking most of the ligands from the 19 ligand data. The correlation between the expected pose Gscore and the pK_d for lobeline AChBP, as well as the correlation between the best Gscore and the pK_d, were highest (albeit still modest) for docking in to this structure.

Glide Gscore as well as other scoring functions available within the Discovery Studio 2.1 suite of software were evaluated for their ability to rank the ligands by K_d values. Although some of the scoring functions showed slightly better correlations (compared to the glide Gscore) between the score and pK_d for docking into the lobeline-aplysia and *lymnaea* hepes structure, these correlations were not significantly better. Refinement of the docked poses using the Schrodinger QPLD protocol, where charges for initially docked poses are recalculated in the protein environment using a quantum mechanical approach, with subsequent redocking and scoring, did provide somewhat better correlations. The results reported here underscore the limitations of rigid docking methodologies and underscore the limitations of current scoring functions which do not adequately account for cation-π interactions.

Future Studies

The Gscore correlation with pK_d was poor and there was no promising correlation between any other scoring function, except for the Aplysia lobeline AChBP structure and

the QPLD Gscore and Coulomb van der Waals energy. However, the K_d values were obtained from different labs using different techniques. Once the best Gscore vs. pK_d was graphed for the ligands docked into the lobeline structure where the K_d values were obtained from the same lab using the same technique, the correlation improved greatly. Therefore, future docking studies measuring the correlation between scoring functions and pK_d values should be done with K_d values obtained using the same technique and from the same lab. Furthermore, one could design a scoring function that picks up cation-π interactions and look for a correlation between the scores and the pK_d. Also, one could "train" a specific scoring function to the K_d values available. Once a good correlation between the score and the K_d values are obtained, one can build a NNR homology model using the co-crystal structure that gave the best correlation and then test it with the 19 ligands data set.

REFERENCES

1. Romanelli, M.; Gratteri, P.; Guandalini, L.; Martini, E.; Bonaccini, C.; Gualtieri, F., Central nicotinic receptors: structure, function, ligands, and therapeutic potential. *ChemMedChem* **2007,** *2* (6), 746-67.

2. Dellisanti, C.; Yao, Y.; Stroud, J.; Wang, Z.; Chen, L., Crystal structure of the extracellular domain of nAChR alpha1 bound to alpha-bungarotoxin at 1.94 A resolution. *Nat Neurosci* **2007,** *10* (8), 953-62.

3. Unwin, N., Refined Structure of the Nicotinic Acetylcholine Receptor at 4 A Resolution. *Journal of Molecular Biology* **2005,** *346* (4), 967-989.

4. Celie, P.; van Rossum-Fikkert, S.; van Dijk, W.; Brejc, K.; Smit, A.; Sixma, T., Nicotine and carbamylcholine binding to nicotinic acetylcholine receptors as studied in AChBP crystal structures. *Neuron* **2004,** *41* (6), 907-14.

5. Hansen, S.; Sulzenbacher, G.; Huxford, T.; Marchot, P.; Taylor, P.; Bourne, Y., Structures of Aplysia AChBP complexes with nicotinic agonists and antagonists reveal distinctive binding interfaces and conformations. *EMBO J* **2005,** *24* (20), 3635-46.

6. Mudo, G.; Belluardo, N.; Fuxe, K., Nicotinic receptor agonists as neuroprotective/neurotrophic drugs. Progress in molecular mechanisms. *J Neural Transm* **2007,** *114* (1), 135-47.

7. Di Angelantonio, S.; Giniatullin, R.; Costa, V.; Sokolova, E.; Nistri, A., Modulation of neuronal nicotinic receptor function by the neuropeptides CGRP and substance P on autonomic nerve cells. *Br J Pharmacol* **2003,** *139* (6), 1061-73.

8. Guo, X.; Lester, R., Ca2+ flux and signaling implications by nicotinic acetylcholine receptors in rat medial habenula. *J Neurophysiol* **2007,** *97* (1), 83-92.

9. Mazurov, A.; Hauser, T.; Miller, C., Selective alpha7 nicotinic acetylcholine receptor ligands. *Curr Med Chem* **2006,** *13* (13), 1567-84.

10. Bencherif, M.; Schmitt, J., Targeting neuronal nicotinic receptors: a path to new therapies. *Curr Drug Targets CNS Neurol Disord* **2002,** *1* (4), 349-57.

11. Breining, S. R.; Mazurov, A. A.; Miller, C. H.; Annette M. Doherty, M. G. B. M. C. D. J. O. J. J. P. A. S. D. W. a. H. Y., Neuronal Nicotinic Acetylcholine Receptor Modulators: Recent Advances and Therapeutic Potential. In *Annual Reports in Medicinal Chemistry*, Academic Press: 2005; Vol. Volume 40, pp 3-16.

12. Szarecka, A.; Xu, Y.; Tang, P., Dynamics of heteropentameric nicotinic acetylcholine receptor: implications of the gating mechanism. *Proteins* **2007,** *68* (4), 948-60.

13. Brejc, K.; van Dijk, W.; Klaassen, R.; Schuurmans, M.; van Der Oost, J.; Smit, A.; Sixma, T., Crystal structure of an ACh-binding protein reveals the ligand-binding domain of nicotinic receptors. *Nature* **2001,** *411* (6835), 269-76.

14. Celie, P.; Klaassen, R.; van Rossum-Fikkert, S.; van Elk, R.; van Nierop, P.; Smit, A.; Sixma, T., Crystal structure of acetylcholine-binding protein from Bulinus truncatus reveals the conserved structural scaffold and sites of variation in nicotinic acetylcholine receptors. *J Biol Chem* **2005,** *280* (28), 26457-66.

15. Bouzat, C.; Gumilar, F.; Spitzmaul, G.; Wang, H.; Rayes, D.; Hansen, S.; Taylor, P.; Sine, S., Coupling of agonist binding to channel gating in an ACh-binding protein linked to an ion channel. *Nature* **2004,** *430* (7002), 896-900.

16. Schmitt, J. D.; Sharples, C. G. V.; Caldwell, W. S., Molecular Recognition in Nicotinic Acetylcholine Receptors: The Importance of π-Cation Interactions. *J. Med. Chem.* **1999,** *42* (16), 3066-3074.

17. Artali, R.; Bombieri, G.; Meneghetti, F., Docking of 6-chloropyridazin-3-yl derivatives active on nicotinic acetylcholine receptors into molluscan acetylcholine binding protein (AChBP). *Farmaco* **2005,** *60* (4), 313-20.

18. Talley, T.; Yalda, S.; Ho, K.; Tor, Y.; Soti, F.; Kem, W.; Taylor, P., Spectroscopic analysis of benzylidene anabaseine complexes with acetylcholine binding proteins as models for ligand-nicotinic receptor interactions. *Biochemistry* **2006,** *45* (29), 8894-902.

19. Taylor, P.; Talley, T.; Radic', Z.; Hansen, S.; Hibbs, R.; Shi, J., Structure-guided drug design: conferring selectivity among neuronal nicotinic receptor and acetylcholine-binding protein subtypes. *Biochem Pharmacol* **2007,** *74* (8), 1164-71.

20. Celie, P.; Kasheverov, I.; Mordvintsev, D.; Hogg, R.; van Nierop, P.; van Elk, R.; van Rossum-Fikkert, S.; Zhmak, M.; Bertrand, D.; Tsetlin, V.; Sixma, T.; Smit, A., Crystal structure of nicotinic acetylcholine receptor homolog AChBP in complex with an alpha-conotoxin PnIA variant. *Nat Struct Mol Biol* **2005,** *12* (7), 582-8.

21. Friesner, R. A.; Banks, J. L.; Murphy, R. B.; Halgren, T. A.; Klicic, J. J.; Mainz, D. T.; Repasky, M. P.; H., K. E.; Shelley, M.; K., P. J.; Shaw, D. E.; Francis, P.; and Shenkin, P. S., Glide: A New Approach for Rapid, Accurate Docking and Scoring. 1. Method and Assessment of Docking Accuracy. *J. Med. Chem.* **2004,** *47* (7), 1739-1749.

22. Accelrys, Inc. *Discovery Studio 2.1*. San Diego, California.

23. Schrodinger. *Glide 5.0.* San Diego, California.

APPENDIX DISTANCES MEASURED

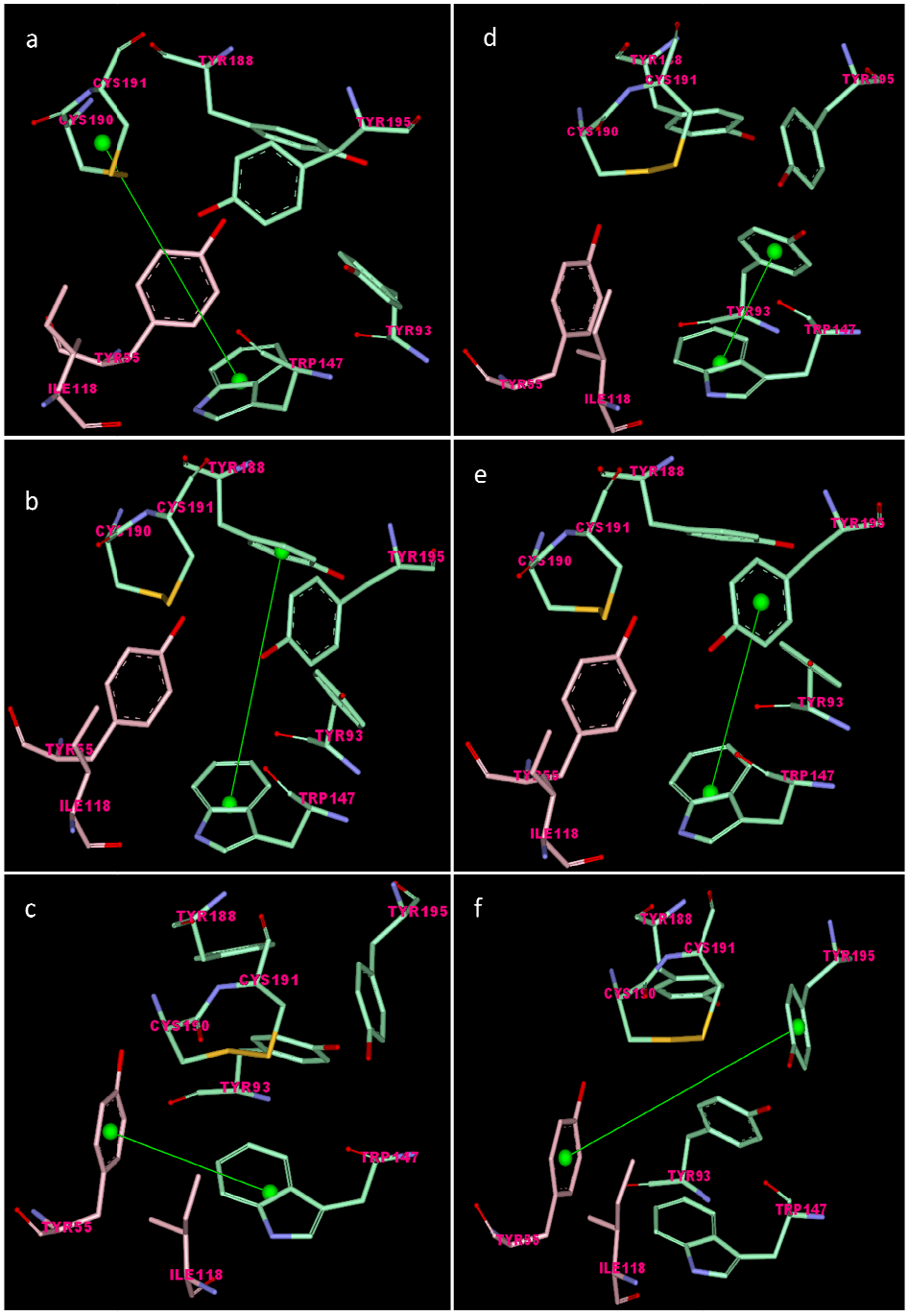

Figure 25. Distances Measured—Complementary to Figure 9. The bright green lines show the distances measured and the bright green spheres are centroids of the ring that they are in.